

Pathways to equilibrium orientation fluctuations in finite stripe-forming systems

Christian Riesch, Günter Radons, and Robert Magerle

Institut für Physik, Technische Universität Chemnitz, D-09107 Chemnitz, Germany

(Received 25 August 2017; published 28 November 2017)

Small-angle orientation fluctuations in ordered stripe-forming systems free of topological defects can exhibit aging and anisotropic growth of two length scales. In infinitely extended systems, the stripe orientation field develops a dominant modulation length $\lambda_{\parallel}^*(t)$ in the direction parallel to the stripes, which increases with time t as $\lambda_{\parallel}^*(t) \sim t^{1/4}$. Simultaneously, the orientation correlation length $\xi_{\perp}(t)$ in the direction perpendicular to the stripes increases as $\xi_{\perp}(t) \sim t^{1/2}$ [Riesch *et al.*, *Interface Focus* **7**, 20160146 (2017)]. Here we show that finite systems of size $L_{\perp} \times L_{\parallel}$ with periodic boundary conditions reach equilibrium when the dominant modulation length $\lambda_{\parallel}^*(t)$ reaches the system size L_{\parallel} in the stripe direction. The equilibration time $\tau_{\text{eq}}^{\parallel}$ is solely determined by L_{\parallel} , with $\tau_{\text{eq}}^{\parallel} \sim L_{\parallel}^4$. In systems with $L_{\perp} < L_{\parallel}^2/2\pi\lambda_p$, where λ_p is the undulation penetration length, the initial aging and coarsening dynamics changes at the crossover time $\tau_c^{\perp} \sim L_{\perp}^2$ to an aging and coarsening dynamics described by the one-dimensional Mullins-Herring equation, before reaching equilibrium at τ_{eq}^{\perp} . Our work reveals the two pathways to equilibrium in stripe phases with periodic boundary conditions, the finite-size scaling behavior of equilibrium orientation fluctuations, and the characteristic exponents associated with the influence of a finite system size.

DOI: [10.1103/PhysRevE.96.052224](https://doi.org/10.1103/PhysRevE.96.052224)

I. INTRODUCTION

Stripe patterns occur in many physical systems, such as thin magnetic films [1–4], Rayleigh-Bénard convection [5,6], and thin films of cylinder-forming block copolymers [7]. A periodic, two-dimensional (2D) stripe pattern is a conceptually simple prototype of more complex modulated phases [8], such as the three-dimensional periodic patterns of lamellae, cylinders, and spheres, as well as the gyroid phase found in block copolymers [9] and surfactant phases [10,11]. In particular, lamellar phases are found in a multitude of physical systems, for instance, smectic liquid crystals [12], lipid membranes [13], and electronic phases in superconductors [14,15].

Orientation fluctuations, due to either thermal noise or a stochastically fluctuating external parameter, are an intrinsic property of any modulated phase. With computer simulations based on a minimal phase-field model (model B with Coulomb interactions), we discovered the aging and coarsening of small-angle orientation fluctuations in ordered stripe-forming systems free of topological defects [16]. The aging and coarsening dynamics is explained [17] by an analytic theory based on the linear elastic model for stripe displacements first introduced by Peierls [18] and Landau [19]: Under the influence of noise, stripes that are initially perfectly ordered develop small-angle orientation fluctuations, and the stripe orientation field is characterized by a dominant modulation length $\lambda_{\parallel}^*(t)$ in the direction parallel to the stripes, which increases with time t as $\lambda_{\parallel}^*(t) \sim t^{1/4}$. Simultaneously, the time-dependent orientation correlation length perpendicular to the stripes $\xi_{\perp}(t)$ increases as $\xi_{\perp}(t) \sim t^{1/2}$.

The orientation fluctuations in stripe phases are to some extent similar to the director fluctuations of layers in smectic liquid crystals, which have been extensively studied both theoretically and experimentally [12,20]. Smectic liquid crystals display the Landau-Peierls instability [18,19,21], which manifests itself as a logarithmic divergence of mean-square displacement fluctuations in three dimensions. The thermally

excited equilibrium fluctuations can lead to the so-called undulation instability if a magnetic field (Helfrich-Hurault effect [22,23]) or mechanical tension [24,25] is applied. For an overview of the different types of undulation phenomena in liquid crystals, we refer to de Gennes' book [12]. In stripe phases, mean-square displacement fluctuations diverge with a power law; however, the mean-square of the orientation fluctuations remains finite, as Toner and Nelson have shown [26]. Nevertheless, infinite stripe phases display aging and coarsening (divergence) of length scales characterizing the orientation field as described above [16,17].

Here we study the influence of periodic boundary conditions on the aging and coarsening dynamics of orientation fluctuations in stripe phases. We consider the inherent anisotropy of the stripe pattern and study finite systems of size $L_{\perp} \times L_{\parallel}$ with periodic boundary conditions where L_{\perp} and L_{\parallel} are the system's extensions in the directions perpendicular and parallel to the stripes, respectively. Utilizing numerical simulations based on a phase-field model and with an analytic theory based on the Landau-Peierls model, we find that these finite systems reach equilibrium when the dominant modulation length $\lambda_{\parallel}^*(t)$ in the direction parallel to the stripes reaches the system size L_{\parallel} . As a consequence, the growth of the orientation correlation length $\xi_{\perp}(t)$ in the direction perpendicular to the stripes stops at the equilibrium correlation length $\xi_{\perp}^{\text{eq}} < L_{\perp}$, if L_{\perp} is large enough. Our analytical calculations based on the Landau-Peierls model reveal the two pathways to equilibrium as well as the scaling forms and characteristic exponents associated with the influence of a finite system size.

Finite-size scaling first emerged as a concept in the study of equilibrium phase transitions in finite systems [27]. Later, it became an important tool for interpreting computer simulations where accessible system sizes are still much smaller than macroscopic samples [28,29]. Scaling concepts in different forms have also proven essential for understanding systems out of equilibrium. Domain growth in phase-ordering systems after a quench [30,31] is one example where finite-size scaling has been studied extensively [32–38]. Recently, the

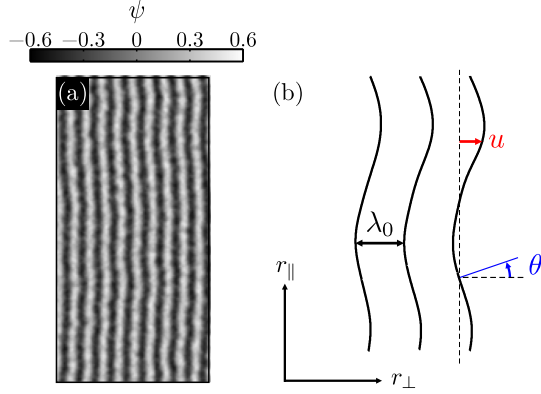


FIG. 1. (a) Snapshot of an ordered stripe-forming system displaying orientation fluctuations. The concentration field $\psi(\mathbf{r}, t = 5 \times 10^5)$ is shown for a noise strength $\eta/\eta_c = \frac{1}{3}$. The image shows a portion of the $55\lambda_0 \times 55\lambda_0$ large simulation area. (b) Illustration of the stripe displacement u and the stripe orientation θ . The thick black lines represent the center lines of individual stripes, while the dashed line indicates $u = 0$. λ_0 indicates the wavelength of the stripe pattern. Adapted from Ref. [17].

system size's influence on the aging behavior of such a system has also been investigated [39]. In the context of stripe-forming systems, the dependence of the orientational susceptibility on the system size has been used to test theoretical results concerning the nature of phase transitions in systems with different interactions [40]. Finite-size scaling is also inherent in a different class of nonequilibrium systems, namely, roughening surfaces and interfaces [41]. In this scenario, the roughness of a surface scales as a power of the system size, as expressed by the Family-Vicsek scaling [42]. In the present work, we will exploit the analogy of the stripe-forming system with the one-dimensional (1D) Mullins-Herring equation as already demonstrated in Ref. [17].

Let us begin by introducing the phenomenology of an ordered stripe-forming system under the influence of noise, where the noise strength η is well below the critical noise strength $\eta_c = 0.020(3)$, which marks an order-disorder transition [16]. Figure 1(a) shows a snapshot of the concentration field $\psi(\mathbf{r}, t)$ for the time $t = 5 \times 10^5$. Starting from an initially unperturbed stripe pattern at $t = 0$ that minimizes the system's free energy, the system evolved according to a Langevin equation (model B with Coulomb interactions) and developed small-angle orientation fluctuations but no topological defects [16]. In a further reduced elastic model, only the coarse-grained displacements of the stripes' center positions are considered. The sketch in Fig. 1(b) introduces the stripe displacement $u(\mathbf{r}, t)$ and the stripe orientation $\theta(\mathbf{r}, t)$, as well as the coordinates r_\perp (perpendicular to the stripes) and r_\parallel (parallel to the stripes). The corresponding extensions of the system are designated L_\perp and L_\parallel , respectively. Due to the anisotropic nature of an ordered stripe pattern, finite systems with different geometries arise. The simplest approach is to consider a square system with $L_\perp = L_\parallel$. Otherwise, only one side can be made small while keeping the other one large. This results in a rectangular geometry, which either contains numerous short stripes ($L_\perp \gg L_\parallel$), or only a few but long stripes ($L_\perp \ll L_\parallel$).

We investigate these different configurations using both numerical simulations and analytical theory. To this end, we closely follow our previous work [16,17], where we studied infinitely extended systems. In the present work, we derive the corresponding expressions that take the system's periodic boundary conditions into account. In Sec. II we introduce the phase-field model for the stripe dynamics, the spatio-temporal correlation functions of the local stripe orientation $\theta(\mathbf{r}, t)$, and the corresponding structure factor. In Sec. III we introduce the Landau-Peierls model for stripe displacement and derive the expressions for the structure factor, the two-time correlation function, and the spatial correlation function of the local stripe orientation. In Sec. IV the numerical results are shown and compared with the analytical expressions derived from the Landau-Peierls model. First, we discuss the case of short stripes, where $L_\perp \gg L_\parallel$, as this is the most pronounced situation leading to equilibrium. Then we discuss the opposite case of long stripes, namely, $L_\perp \ll L_\parallel$, where the system displays a quasi-1D behavior. Finally, we discuss the pathway to equilibrium for finite square systems with $L_\perp = L_\parallel$ and summarize our results in Sec. V.

II. PHASE-FIELD MODEL FOR STRIPE DYNAMICS

A. Free energy and stochastic equation

We performed numerical simulations of a minimal model for stripe formation and dynamics, known as model B with Coulomb interactions. The model is based on the dynamic equation for phase separation with a conserved order parameter [43]:

$$\partial_t \psi(\mathbf{r}, t) = \nabla^2 \frac{\delta \mathcal{F}[\psi]}{\delta \psi(\mathbf{r}, t)} + \zeta(\mathbf{r}, t), \quad (1)$$

where $\psi(\mathbf{r}, t)$ is a scalar field representing the concentration difference $\psi(\mathbf{r}, t) = \psi_A(\mathbf{r}, t) - \psi_B(\mathbf{r}, t)$ between two components A and B . The Gaussian noise term $\zeta(\mathbf{r}, t)$ satisfies $\langle \zeta(\mathbf{r}, t) \rangle = 0$ and $\langle \zeta(\mathbf{r}, t) \zeta(\mathbf{r}', t') \rangle = -2\eta \nabla^2 \delta(\mathbf{r} - \mathbf{r}') \delta(t - t')$, where $\langle \cdot \rangle$ stands for the statistical average and η parameterizes the noise strength. The free-energy functional $\mathcal{F}[\psi(\mathbf{r}, t)]$ was first derived by Ohta and Kawasaki [44]. In d spatial dimensions,

$$\mathcal{F}[\psi] = \int \{-\psi(\mathbf{r}', t)^2 + \psi(\mathbf{r}', t)^4 + [\nabla \psi(\mathbf{r}', t)]^2\} d^d r' + \frac{\Gamma}{2} \iint \psi(\mathbf{r}', t) G(\mathbf{r}' - \mathbf{r}'') \psi(\mathbf{r}'', t) d^d r' d^d r'', \quad (2)$$

where the first integral is a short-range Ginzburg-Landau free energy, and the second integral represents repulsive long-range Coulomb interactions controlled by the parameter Γ . The Green's function $G(\mathbf{r} - \mathbf{r}')$ is defined by $-\nabla^2 G(\mathbf{r} - \mathbf{r}') = \delta(\mathbf{r} - \mathbf{r}')$. Inserting the free energy [Eq. (2)] into the dynamic equation [Eq. (1)] yields the following stochastic partial differential equation (PDE):

$$\partial_t \psi(\mathbf{r}, t) = \nabla^2 [-\psi(\mathbf{r}, t) + \psi^3(\mathbf{r}, t) - \nabla^2 \psi(\mathbf{r}, t)] - \Gamma \psi(\mathbf{r}, t) + \zeta(\mathbf{r}, t). \quad (3)$$

Compared to more sophisticated approaches for simulating block copolymers [45,46], the model given by Eq. (3) has the

advantage of being computationally less demanding, which enables us to more easily investigate its long-term behavior.

As detailed in our previous works [16,17], we prepare the system in a perfectly ordered state consisting of parallel stripes with wavelength $\lambda_0 = 2\pi\Gamma^{-\frac{1}{4}}$. The amplitude and wavelength were chosen to minimize the free energy $\mathcal{F}[\psi]$ in a single-mode approximation [47]. We fix the interaction parameter Γ as 0.2, for which Eq. (3) exhibits stripe formation [48]. The noise strength η was chosen so that $\eta/\eta_c = \frac{1}{30}$, well below the critical noise strength $\eta_c = 0.020(3)$, at which an order-disorder transition occurs [16]. Using an efficient pseudospectral algorithm [49], we performed simulations of Eq. (3) with periodic boundary conditions in $d = 2$ dimensions on lattices with size $L_\perp \times L_\parallel$. Space and time were discretized in increments of $\Delta r = \lambda_0/10$ and $\Delta t = 0.1$, respectively. The results presented below were averaged over 40 independent realizations. The quantities which have been computed in equilibrium (with subscript or superscript “eq”) were additionally averaged over times $t > 10^5$ ($t > 10^6$ for $L_\parallel = 16\lambda_0$).

B. Correlation functions

Our main observable is the local stripe orientation $\theta(\mathbf{r}, t)$, computed from the concentration field $\psi(\mathbf{r}, t)$ by using the gradient-square tensor [50–52]. Some examples for the orientation fields $\theta(\mathbf{r}, t)$ of finite-size systems in equilibrium are presented in Fig. 2(a). A visual inspection of the figure suggests substantial differences regarding the orientation fluctuations. These differences become even clearer when considering the coarse-grained orientation field, where structures smaller than one wavelength λ_0 have been removed using a Gaussian filter [Fig. 2(b)]. The magnitude of the orientation fluctuations is largest in the system containing long stripes [Fig. 2(b), top left], whereas fluctuations with a wavelength $> \lambda_0$ are much less pronounced in systems where L_\parallel is small [Fig. 2(b), bottom left and right]. The small square system [Fig. 2(b), bottom left] exhibits a modulation of the orientation field in the stripe direction, with the dominant wavelength $\lambda_\parallel^* = L_\parallel$ spanning the whole extent of the system parallel to the stripes, whereas almost no variation is seen in the perpendicular direction. The latter also holds for the system where $L_\perp \ll L_\parallel$ [Fig. 2(b), top left]. In contrast, in the large square system [Fig. 2(b), top right], there is a certain degree of variation perpendicular to the stripes. This is also the case for the system where $L_\perp \gg L_\parallel$ [Fig. 2(b), bottom right]. However, the spatial extent of the orientational domains in the direction perpendicular to the stripes does not reach the system size L_\perp .

To investigate the dynamics of the stripe orientation $\theta(\mathbf{r}, t)$, we use spatio-temporal correlation functions. The most general form is given by

$$C_\theta(\mathbf{r}, \mathbf{r}', t, t_w) \equiv \text{Re} \left[\left\langle e^{2i[\theta(\mathbf{r}, t) - \theta(\mathbf{r}', t_w)]} \right\rangle_\zeta - \left\langle e^{2i\theta(\mathbf{r}, t)} \right\rangle_\zeta \left\langle e^{-2i\theta(\mathbf{r}', t_w)} \right\rangle_\zeta \right], \quad (4)$$

which takes into account the symmetry and periodicity of the stripe orientation, namely, its invariance under the transformation $\theta \rightarrow \theta + \pi$. In the case of spatial translation invariance, Eq. (4) depends only on the difference $\mathbf{R} \equiv \mathbf{r} - \mathbf{r}'$ and can thus be written as $C_\theta(\mathbf{R}, t, t_w) \equiv C_\theta(\mathbf{r}, \mathbf{r} + \mathbf{R}, t, t_w)$. Furthermore, in a finite system with periodic boundary conditions, the

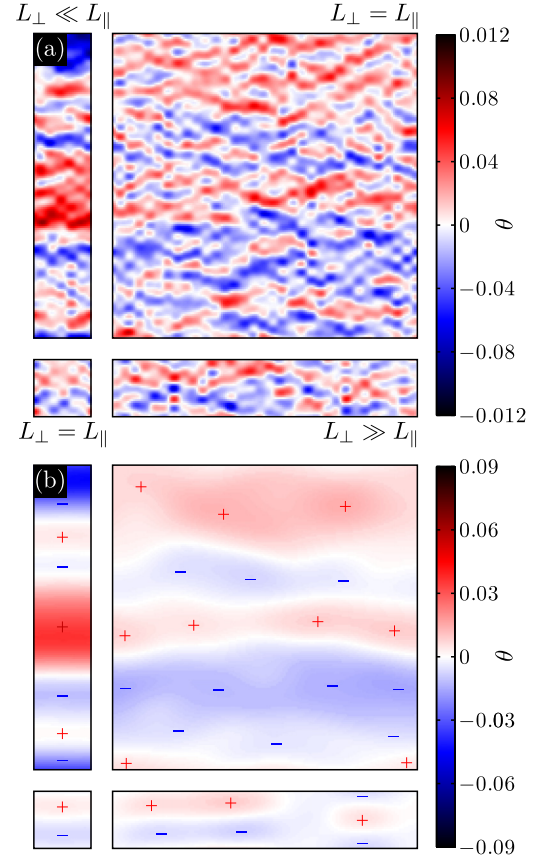


FIG. 2. (a) Examples of orientation fields $\theta(\mathbf{r}, t)$ for stripe-forming systems with different extensions L_\perp and L_\parallel . The dynamics was advanced until equilibrium was attained. Top left: $L_\perp = 3\lambda_0$, $L_\parallel = 16\lambda_0$. Top right: $L_\perp = L_\parallel = 16\lambda_0$. Bottom left: $L_\perp = L_\parallel = 3\lambda_0$. Bottom right: $L_\perp = 16\lambda_0$, $L_\parallel = 3\lambda_0$. (b) Orientation fields from the same systems as in (a) where fluctuations smaller than λ_0 were removed. The orientation angle in the two bottom panels was multiplied by a factor of three.

correlation function is also periodic in the system size: $C_\theta(\mathbf{R}, t, t_w) \equiv C_\theta[\mathbf{R} + (mL_\perp, nL_\parallel), t, t_w]$, with integers m, n . From this quantity, the two-time correlation function $C_\theta(t, t_w)$ is obtained by setting $\mathbf{R} = \mathbf{0}$:

$$C_\theta(t, t_w) \equiv C_\theta(\mathbf{R} = \mathbf{0}, t, t_w). \quad (5)$$

Conversely, the equal-time spatial correlation function is given by

$$C_\theta(\mathbf{R}, t) \equiv C_\theta(\mathbf{R}, t, t_w = t). \quad (6)$$

We also consider a related quantity, the structure factor of the orientation, $S_\theta(\mathbf{q}, t)$, which is given by the Fourier transform of the equal-time spatial orientation correlation function:

$$S_\theta(\mathbf{q}, t) \equiv \int_0^{L_\perp} \int_0^{L_\parallel} C_\theta(\mathbf{R}, t) e^{-i\mathbf{q}\cdot\mathbf{R}} d^2R. \quad (7)$$

Here the wave vector $\mathbf{q} \equiv (q_m^\perp, q_n^\parallel) \equiv 2\pi(m/L_\perp, n/L_\parallel)$, with integers m, n satisfying $-\infty \leq m, n \leq +\infty$. The structure factor parallel to the stripes $S_\theta(q_m^\perp = 0, q_n^\parallel, t)$ exhibits a

characteristic maximum at a wave number $q_{\parallel}^*(t) \equiv \arg \max_{q_{\parallel}} S_{\theta}(0, q_{\parallel}, t)$, where the peak intensity $S_{\theta}^*(t) \equiv S_{\theta}(0, q_{\parallel}^*, t)$. Numerically, we first fit smoothing splines to $S_{\theta}(0, q_{\parallel}, t)$ before calculating $q_{\parallel}^*(t)$. The corresponding wavelength $\lambda_{\parallel}^*(t) \equiv 2\pi/q_{\parallel}^*(t)$ is referred to as the dominant modulation length.

For small angles θ , such as those observed at small noise strengths $\eta \ll \eta_c$, the orientation correlation function [Eq. (4)] simplifies to $C_{\theta}(\mathbf{r}, \mathbf{r}', t, t_w) \simeq 4[(\theta(\mathbf{r}, t)\theta(\mathbf{r}', t_w))_{\zeta} - \langle \theta(\mathbf{r}, t) \rangle_{\zeta} \langle \theta(\mathbf{r}', t_w) \rangle_{\zeta}]$. We will use this approximation in our analytical calculations presented below.

III. LANDAU-PEIERLS MODEL FOR STRIPE DISPLACEMENT

A. Free energy and stochastic equation

In this section, we discuss a model for smectic liquid crystals [12] in $d = 3$ dimensions and stripe-forming systems ($d = 2$) which dates back to works by Peierls [18] and Landau [19]. Later the theory was developed by de Gennes [53] for smectic liquid crystals and investigated in two dimensions for stripe phases as well by Toner and Nelson [26]. Specifically, the static structure factor and the spatial correlation function of the displacement field were computed [26,54]. The model is defined in terms of a displacement field $u(\mathbf{r}, t)$, which indicates the distance between a stripe (a layer in $d = 3$) and its unperturbed position [see Fig. 1(a)]. It has been shown that both smectics and stripe-forming systems can be described by the free-energy functional [26,55,56]

$$\mathcal{F}_{\text{el}}[u] = \frac{1}{2} \int d^2 r' \{v_2 [\partial_{\perp} u(\mathbf{r}', t)]^2 + v_4 [\partial_{\parallel}^2 u(\mathbf{r}', t)]^2\}, \quad (8)$$

where $u(\mathbf{r}, t)$ represents the displacement field and $v_2, v_4 > 0$ are elastic constants related to compression and bending (splay), respectively. The operators ∂_{\perp} and ∂_{\parallel} represent the partial derivatives with respect to r_{\perp} and r_{\parallel} , respectively. Equation (8) can be derived from the phase-field model for the stripe-forming system given by Eq. (3) by using a single-mode approximation for the concentration field $\psi(\mathbf{r}, t) = A_0 \cos(q_0 r_{\perp})$, linearizing the term involving $\psi^3(\mathbf{r}, t)$, and neglecting higher-order terms in $u(\mathbf{r}, t)$ [56,57]. In our case, the elastic constants assume the values $v_2 = 4\sqrt{\Gamma} = 4q_0^2$ and $v_4 = 1$, implying that the so-called penetration length of undulation fluctuations [58] $\lambda_p \equiv \sqrt{v_4/v_2} = \lambda_0/4\pi$. We now consider the stochastic PDE

$$\begin{aligned} \partial_t u(\mathbf{r}, t) &= -\frac{\delta \mathcal{F}_{\text{el}}[u]}{\delta u(\mathbf{r}, t)} + \zeta_u(\mathbf{r}, t) = v_2 \partial_{\perp}^2 u(\mathbf{r}, t) \\ &\quad - v_4 \partial_{\parallel}^4 u(\mathbf{r}, t) + \zeta_u(\mathbf{r}, t), \end{aligned} \quad (9)$$

where the correlations of the white noise $\zeta_u(\mathbf{r}, t)$ are given by $\langle \zeta_u(\mathbf{r}, t) \zeta_u(\mathbf{r}', t') \rangle = 2\sigma^2 \delta(\mathbf{r} - \mathbf{r}') \delta(t - t')$, where σ^2 is the noise strength. Equation (9) represents a gradient descent dynamics within the energy \mathcal{F}_{el} combined with the stochastic noise term $\zeta_u(\mathbf{r}, t)$ and thus corresponds to model A in the classification of Hohenberg and Halperin [43].

In the following, we consider all functions as periodic in space with periods L_{\perp} and L_{\parallel} . After introducing the Fourier transform $\hat{u}(\mathbf{q}, t) \equiv \int_0^{L_{\perp}} \int_0^{L_{\parallel}} u(\mathbf{r}, t) e^{-i\mathbf{q}\cdot\mathbf{r}} d^2 r$, with

$\mathbf{q} = (q_{\perp}^{\perp}, q_{\parallel}^{\parallel})$, the equation reads

$$d_t \hat{u}(\mathbf{q}, t) = -a(\mathbf{q}) \hat{u}(\mathbf{q}, t) + \hat{\zeta}_u(\mathbf{q}, t), \quad (10)$$

where the damping rate

$$a(\mathbf{q}) \equiv v_2 (q_{\perp}^{\perp})^2 + v_4 (q_{\parallel}^{\parallel})^4, \quad (11)$$

and the Fourier-transformed noise $\hat{\zeta}_u(\mathbf{q}, t)$ has the following correlations: $\langle \hat{\zeta}_u(\mathbf{q}, t) \hat{\zeta}_u(\mathbf{q}', t') \rangle = 2\sigma^2 L_{\perp} L_{\parallel} \delta_{\mathbf{q}, -\mathbf{q}'} \delta(t - t')$. Since we are mainly interested in the dynamics of the orientation field $\theta(\mathbf{r}, t)$, we follow Toner and Nelson [26] and compute $\theta(\mathbf{r}, t)$ from the displacement field $u(\mathbf{r}, t)$ by taking the derivative in the r_{\parallel} direction [see Fig. 1(a)]: $\theta(\mathbf{r}, t) \equiv -\tan^{-1}[\partial_{\parallel} u(\mathbf{r}, t)] \simeq -\partial_{\parallel} u(\mathbf{r}, t)$, where the latter approximation holds for small gradients of the displacement $\partial_{\parallel} u(\mathbf{r}, t) \ll 1$. Applying this to Eq. (10) leads to the following differential equation for the Fourier transform $\hat{\theta}(\mathbf{q}, t)$ of the orientation field $\theta(\mathbf{q}, t)$:

$$d_t \hat{\theta}(\mathbf{q}, t) \equiv d_t [i q_{\parallel}^{\parallel} \hat{u}(\mathbf{q}, t)] = -a(\mathbf{q}) \hat{\theta}(\mathbf{q}, t) + \hat{\zeta}_{\theta}(\mathbf{q}, t), \quad (12)$$

where the noise ζ_{θ} has correlations $\langle \zeta_{\theta}(\mathbf{r}, t) \zeta_{\theta}(\mathbf{r}', t') \rangle = -2\sigma^2 \partial_{\parallel}^2 \delta(\mathbf{r} - \mathbf{r}') \delta(t - t')$ in real space, which corresponds to $\langle \hat{\zeta}_{\theta}(\mathbf{q}, t) \hat{\zeta}_{\theta}(\mathbf{q}', t') \rangle = 2\sigma^2 L_{\perp} L_{\parallel} (q_{\parallel}^{\parallel})^2 \delta_{\mathbf{q}, -\mathbf{q}'} \delta(t - t')$ in Fourier space. Equation (12) is a linear stochastic ordinary differential equation, similar to those arising in the context of surface roughening processes [59], which are known to exhibit coarsening and aging [31].

B. Structure factor $S_{\theta}(\mathbf{q}, t)$

For the initial condition $\hat{\theta}(\mathbf{q}, t = 0) = 0$, the solution of Eq. (12) can be written as $\hat{\theta}(\mathbf{q}, t) = \int_0^t e^{-a(\mathbf{q})[t-\tau]} \hat{\zeta}_{\theta}(\mathbf{q}, \tau) d\tau$. Inserting this expression into the correlation function

$$S_{\theta}(\mathbf{q}, \mathbf{q}', t, t_w) \equiv 4 \langle \hat{\theta}(\mathbf{q}, t) \hat{\theta}(-\mathbf{q}', t_w) \rangle_{\zeta_{\theta}}, \quad (13)$$

we obtain

$$\begin{aligned} S_{\theta}(\mathbf{q}, \mathbf{q}', t, t_w) &= 4 \int_0^t \int_0^{t_w} e^{-a(\mathbf{q})[t-\tau-t_w-\tau']} \\ &\quad \times \langle \hat{\zeta}_{\theta}(\mathbf{q}, \tau) \hat{\zeta}_{\theta}(-\mathbf{q}', \tau') \rangle d\tau d\tau' \\ &= 8\sigma^2 L_{\perp} L_{\parallel} (q_{\parallel}^{\parallel})^2 \delta_{\mathbf{q}, \mathbf{q}'} e^{-a(\mathbf{q})[t+t_w]} \int_0^{t_w} e^{2a(\mathbf{q})\tau'} d\tau' \\ &= \frac{4\sigma^2 L_{\perp} L_{\parallel} (q_{\parallel}^{\parallel})^2}{a(\mathbf{q})} \delta_{\mathbf{q}, \mathbf{q}'} \{e^{-a(\mathbf{q})[t-t_w]} - e^{-a(\mathbf{q})[t+t_w]}\}, \end{aligned} \quad (14)$$

where the waiting time $t_w \leq t$. We note that the average $\langle \hat{\theta}(\mathbf{q}, t) \rangle_{\zeta_{\theta}}$ vanishes for all times t . By using the spatial translation invariance of the correlation function $C_{\theta}(\mathbf{r}, \mathbf{r} + \mathbf{R}, t, t_w)$ and applying the Wiener-Khintchine theorem [60], the following identity is obtained:

$$S_{\theta}(\mathbf{q}, \mathbf{q}', t, t_w) = L_{\perp} L_{\parallel} \delta_{\mathbf{q}, \mathbf{q}'} S_{\theta}(\mathbf{q}, t, t_w), \quad (15)$$

where $S_{\theta}(\mathbf{q}, t, t_w) \equiv \int_0^{L_{\perp}} \int_0^{L_{\parallel}} e^{-i\mathbf{q}\cdot\mathbf{R}} C_{\theta}(\mathbf{R}, t, t_w) d^2 R$ is the two-time structure factor. A comparison of Eqs. (14) and (15) yields

$$S_{\theta}(\mathbf{q}, t, t_w) = \frac{4\sigma^2 (q_{\parallel}^{\parallel})^2}{a(\mathbf{q})} \{e^{-a(\mathbf{q})[t-t_w]} - e^{-a(\mathbf{q})[t+t_w]}\}. \quad (16)$$

The appearance of $(q_n^\parallel)^2$ in the numerator in Eq. (16) indicates that there are no fluctuations with $q_n^\parallel = 0$. The latter correspond to a pure compression or dilation of the stripe pattern, which does not affect the orientation field. The equal-time structure factor is given by

$$S_\theta(\mathbf{q}, t) = \frac{4\sigma^2(q_n^\parallel)^2}{a(\mathbf{q})} \{1 - e^{-2a(\mathbf{q})t}\}. \quad (17)$$

From this expression, we can immediately read off the characteristic time constants describing the dynamics of spatial orientation fluctuations with wave vectors q_m^\perp and q_n^\parallel . The characteristic times are largest for the smallest wave numbers $q_1^\perp = 2\pi/L_\perp$ and $q_1^\parallel = 2\pi/L_\parallel$ in a given system, corresponding to spatial orientation fluctuations with wavelengths equal to the system's extensions L_\perp and L_\parallel , respectively. We will show below that these time constants determine the pathways to equilibrium: The crossover time

$$\tau_C^\perp \equiv \frac{1}{2\nu_2} (L_\perp/2\pi)^2 \quad (18)$$

and the equilibration time

$$\tau_{\text{eq}}^\parallel \equiv \frac{1}{2\nu_4} (L_\parallel/2\pi)^4 \quad (19)$$

is the time when the system reaches equilibrium. We will show below that in systems with $\tau_C^\perp < \tau_{\text{eq}}^\parallel$, the initial aging and coarsening dynamics changes at τ_C^\perp to the aging and coarsening dynamics of a quasi-1D system. The condition $\tau_C^\perp < \tau_{\text{eq}}^\parallel$ is met by systems with $L_\perp < L_\parallel^2/2\pi\lambda_p$ where λ_p is the undulation penetration length. The interplay of the two characteristic times τ_C^\perp and $\tau_{\text{eq}}^\parallel$ and their dependence on the system size will be a central topic of this work.

From the equal-time structure factor $S_\theta(\mathbf{q}, t)$ [Eq. (17)] in the limit $t \rightarrow \infty$ we obtain the equilibrium structure factor

$$S_\theta^{\text{eq}}(\mathbf{q}) = \frac{4\sigma^2(q_n^\parallel)^2}{\nu_2(q_m^\perp)^2 + \nu_4(q_n^\parallel)^4}. \quad (20)$$

Note that $S_\theta^{\text{eq}}(\mathbf{q})$ has the same \mathbf{q} dependence as the light-scattering intensity in smectic systems derived in Refs. [12,53], because the fluctuations measured in such experiments are director (i.e., orientation) fluctuations. Below we also consider a cut through the equal-time structure factor parallel to the stripes:

$$S_\theta(q_m^\perp = 0, q_n^\parallel, t) = \frac{4\sigma^2}{\nu_4(q_n^\parallel)^2} [1 - e^{-2\nu_4(q_n^\parallel)^4 t}]. \quad (21)$$

The properties of Eq. (21) in an infinite system have been discussed in Ref. [17]. Recapitulating briefly, this function admits the scaling form $S_\theta(q_\perp = 0, q_\parallel, t) \sim t^{2\beta + \frac{1}{z}} \hat{f}(q_\parallel t^{\frac{1}{z}})$, with the exponents $\beta = \frac{1}{8}$ and $z = 4$ determining the universality class [61–63]. The structure factor has a single maximum at the wave number $q_\parallel^*(t) \equiv 2\pi/\lambda^*(t) = \sqrt[4]{\frac{c_0}{2\nu_4 t}}$, which shifts to ever smaller wave numbers as time progresses, while the intensity at the maximum increases as $S_\theta^*(t) \equiv S_\theta^*[0, q_\parallel^*(t), t] = \frac{4\sigma^2}{c_1} \sqrt{\frac{2t}{c_0\nu_4}}$ [17]. The constants $c_0 \equiv -W_{-1}(-\sqrt{e}/2) - 1/2 \approx 1.2564$, where $W_{-1}(\cdot)$ represents the negative branch of the Lambert W function [64], and $c_1 \equiv (1 - e^{-c_0})^{-1} \approx 1.3986$.

C. Two-time correlation function $C_\theta(t, t_w)$

From the two-time structure factor [Eq. (16)], the corresponding two-time correlation function $C_\theta(t, t_w)$ can be obtained by summing over all wave vectors $\mathbf{q} \neq \mathbf{0}$:

$$\begin{aligned} C_\theta(t, t_w) &= \frac{1}{L_\perp L_\parallel} \sum_{m,n} S_\theta(\mathbf{q}, t, t_w) \\ &= \frac{1}{L_\perp L_\parallel} \sum_{m,n} \frac{4\sigma^2(q_n^\parallel)^2}{a(\mathbf{q})} \{e^{-a(\mathbf{q})[t-t_w]} - e^{-a(\mathbf{q})[t+t_w]}\} \\ &\equiv I(t - t_w) - I(t + t_w). \end{aligned} \quad (22)$$

For convenience of notation, we have written $C_\theta(t, t_w)$ as the difference of two functions in Eq. (22). Considering the summation over the allowed wave vectors explicitly yields some insight into the behavior of finite systems, as we will show in Sec. IV. Since Eq. (16) is an even function of both q_m^\perp and q_n^\parallel , we have

$$\begin{aligned} I(t) &= \frac{4\sigma^2}{L_\perp L_\parallel} \left\{ 4 \sum_{m=1}^{\infty} \sum_{n=1}^{\infty} \frac{(q_n^\parallel)^2}{a(\mathbf{q})} e^{-a(\mathbf{q})t} \right. \\ &\quad \left. + 2 \sum_{n=1}^{\infty} \frac{1}{\nu_4(q_n^\parallel)^2} e^{-\nu_4(q_n^\parallel)^4 t} \right\}, \end{aligned} \quad (23)$$

where the second sum over n accounting for the case $m = 0$. The terms with $n = 0$ vanish since q_n^\parallel appears in the numerator in Eq. (22).

D. Spatial correlation function $C_\theta(r_\perp, \mathbf{0}, t)$

In our previous work [17], we investigated the behavior of the spatial correlation function $C_\theta(r_\perp, r_\parallel = 0, t)$ perpendicular to the stripes, which is a special case of the quantity defined in Eq. (6). For an infinite system, we found a growing correlation length and a crossover from a short-range to a power-law decay. Here we focus on the behavior in a finite system. The spatial correlation function perpendicular to the stripes is given by

$$\begin{aligned} C_\theta(r_\perp, r_\parallel = 0, t) &= \frac{1}{L_\perp L_\parallel} \sum_{m,n} S_\theta(\mathbf{q}, t, t) \cos(q_\perp r_\perp) \\ &= \frac{4\sigma^2}{L_\perp L_\parallel} \left\{ 4 \sum_{n=1}^{\infty} \sum_{m=1}^{\infty} \frac{(q_n^\parallel)^2}{a(\mathbf{q})} [1 - e^{-2a(\mathbf{q})t}] \right. \\ &\quad \times \cos(q_m^\perp r_\perp) + 2 \sum_{n=1}^{\infty} \frac{1}{\nu_4(q_n^\parallel)^2} \\ &\quad \left. \times [1 - e^{-2\nu_4(q_n^\parallel)^4 t}] \right\}. \end{aligned} \quad (24)$$

The spatial decay of this function indicates the average extent of orientational domains in the direction perpendicular to the stripes.

IV. RESULTS AND DISCUSSION

A. Short stripes: $L_\perp \gg L_\parallel$

We first consider systems containing many short stripes, where the system size $L_\perp \gg L_\parallel$, while L_\parallel remains small.

In Fig. 3(a) the temporal evolution of the spatial correlation function $C_\theta(r_\perp, r_\parallel = 0, t)$ is shown based on data from a stripe-forming system with $L_\perp = 384\lambda_0$ and $L_\parallel = 8\lambda_0$. Initially the correlation function decays rapidly and exhibits a growing correlation length $\xi_\perp(t)$, closely resembling the behavior of infinite systems [16,17]. However, at late times $t \gtrsim 5 \times 10^3$, $C_\theta(r_\perp, r_\parallel = 0, t)$ reaches equilibrium while still exhibiting small fluctuations around its equilibrium state. This transition is also visible in the time series of the correlation length $\xi_\perp(t)$, plotted in Fig. 3(b) together with the dominant modulation length $\lambda_\parallel^*(t)$, which is extracted from the structure factor $S_\theta(q_m^\perp = 0, q_n^\parallel, t)$ parallel to the stripes. Notably both quantities cross over to a constant value at approximately the same time $\tau_{\text{eq}}^\parallel = \frac{1}{2v_4}(L_\parallel/2\pi)^4$ [Eq. (19)], indicated by a dashed vertical line in Fig. 3(b), namely, the time when $\lambda_\parallel^*(t)$ reaches the system size L_\parallel in the stripe direction. So the system size L_\parallel determines not only the saturation of the modulation length $\lambda_\parallel^*(t)$ parallel to the stripes, but also determines the equilibrium correlation length ξ_\perp^{eq} perpendicular to the stripes.

We note that we used the first moment to determine $\xi_\perp(t)$ from the numerical data: $\xi_\perp(t) \equiv K \int_0^{L_\perp/2} r_\perp C_\theta(r_\perp, 0, t) dr_\perp / \int_0^{L_\perp/2} C_\theta(r_\perp, 0, t) dr_\perp$. With $K = 1$, this method yields the exact correlation length in the case that $C_\theta(r_\perp, 0, t)$ is a purely exponential function. For the numerical evaluation, we chose an empirical value $K = 4.5$ to account for deviations in the numerical data from the purely exponential form.

For $t \lesssim \tau_{\text{eq}}^\parallel$, the growth of $\lambda_\parallel^*(t)$ and $\xi_\perp(t)$ is described by the growth laws for infinite systems [17], namely, $\lambda_\parallel^*(t) = 2\pi\sqrt[4]{2v_4t/c_0}$ and $\xi_\perp(t) = \sqrt{8v_2t}$ [red lines in Fig. 3(b)]. To further characterize the dynamics, we compute the two-time correlation function $C_\theta(t, t_w)$, shown in Fig. 3(c) for a system with $L_\perp = 384\lambda_0$ and $L_\parallel = 3\lambda_0$. Plotted as a function of $t - t_w$, $C_\theta(t, t_w)$ exhibits a rapid decay which resembles an exponential [cf. the inset in Fig. 3(b)]. Most importantly, the two-time correlation function does not depend on the waiting time t_w : it is time-translationally invariant. This is a clear indication that the system is in equilibrium for $t \gtrsim \tau_{\text{eq}}^\parallel$, where $\tau_{\text{eq}}^\parallel = 2.025 \times 10^2$ for $L_\parallel = 3\lambda_0$.

To explain these numerical results, we calculate the corresponding correlation functions of the Landau-Peierls model, starting with the spatial correlation function $C_\theta(r_\perp, r_\parallel = 0, t)$ given in Eq. (24). In the limit $L_\perp \rightarrow \infty$, we may replace the sum $\frac{1}{L_\perp} \sum_m$ by the integral $\frac{1}{2\pi} \int dq_\perp$, which leads to

$$C_\theta(r_\perp, r_\parallel = 0, t) = \frac{2\sigma^2}{L_\parallel \sqrt{v_2 v_4}} \sum_{n=1}^{\infty} \left\{ e^{-(q_n^\parallel)^2 \lambda_p r_\perp} + e^{-(q_n^\parallel)^2 \lambda_p r_\perp} \operatorname{erf} \left[\sqrt{2v_4 t} (q_n^\parallel)^2 - \frac{r_\perp}{\sqrt{8v_2 t}} \right] - e^{(q_n^\parallel)^2 \lambda_p r_\perp} \operatorname{erfc} \left[\sqrt{2v_4 t} (q_n^\parallel)^2 + \frac{r_\perp}{\sqrt{8v_2 t}} \right] \right\}, \quad (25)$$

with the undulation penetration length $\lambda_p \equiv \sqrt{v_4/v_2}$. The red lines in Fig. 3(a) represent Eq. (25), with the sum truncated after 10^5 terms. It was evaluated at the same times as the numerical data. The best fit for the numerical data is obtained

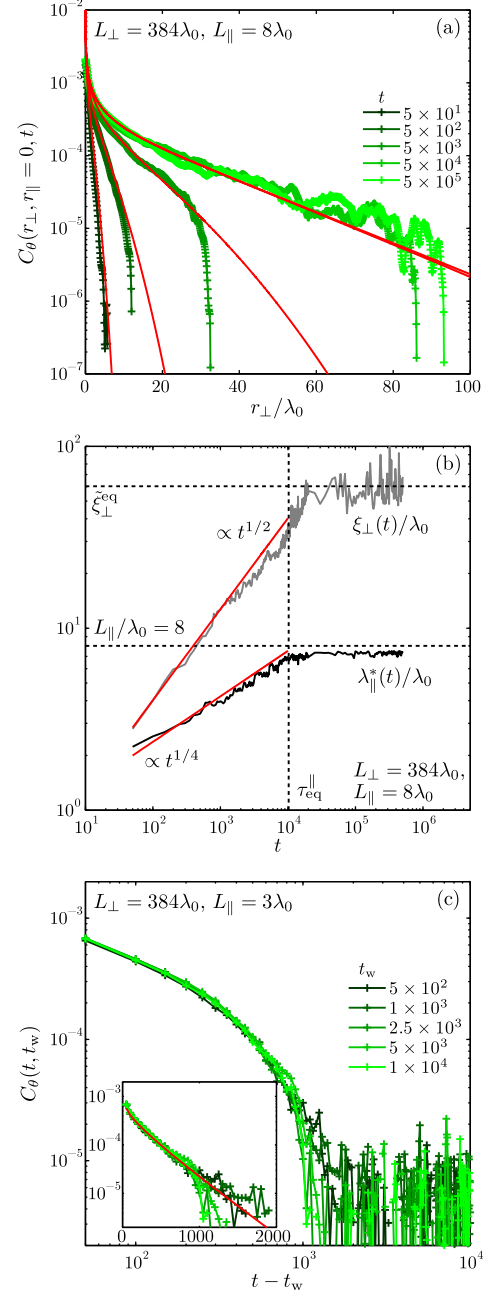


FIG. 3. Pathway to equilibrium in systems comprised of short stripes. (a) Temporal evolution of the spatial correlation function $C_\theta(r_\perp, r_\parallel = 0, t)$ for $L_\perp = 384\lambda_0$ and $L_\parallel = 8\lambda_0$. The solid red lines represent the analytical result of Eq. (25) at the same times. The curves for $t = 5 \times 10^4$ and 5×10^5 overlap each other, indicating that the coarsening has stopped. (b) Growing length scales $\xi_\perp(t)$ and $\lambda_\parallel^*(t)$ extracted from the same system as shown in (a). In the log-log plot, the crossover from an algebraic increase to a constant value at the equilibration time $\tau_{\text{eq}}^\parallel$ [Eq. (19)] is clearly visible. The lower horizontal line represents the system size L_\parallel , which limits $\lambda_\parallel^*(t)$. $\xi_\perp(t)$ approaches the equilibrium correlation length ξ_\perp^{eq} [derived from Eq. (27)], indicated by the upper horizontal line. (c) Equilibrium dynamics of the two-time correlation function in a system with $L_\perp = 384\lambda_0$ and $L_\parallel = 3\lambda_0$. For the range of times shown here, $C_\theta(t, t_w)$ only depends on the difference $t - t_w$. In the inset, the same data are shown in a semilogarithmic plot. The solid red line is the theoretical result given in Eq. (28).

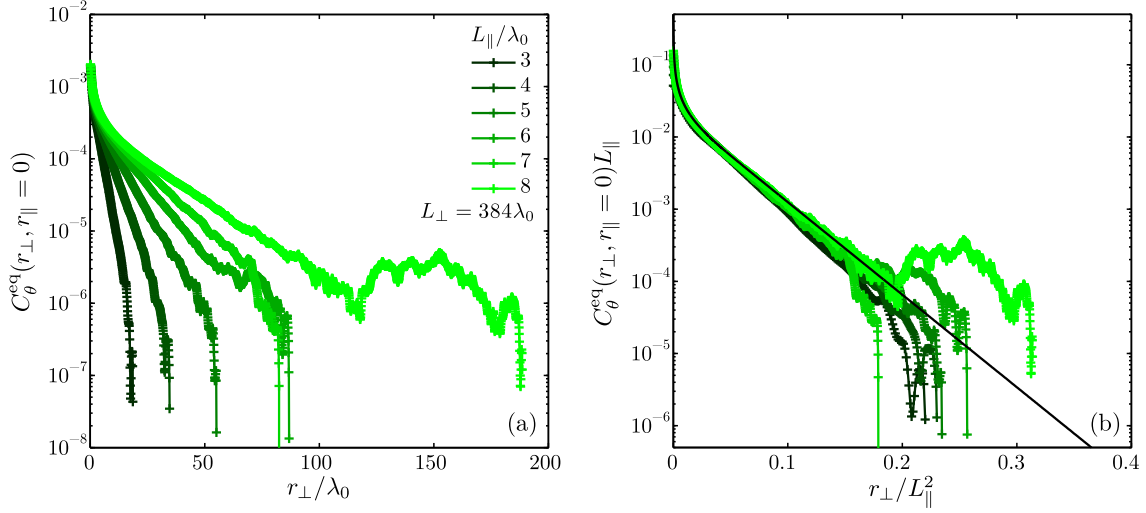


FIG. 4. Scaling behavior of the equilibrium spatial orientation correlation function $C_\theta^{\text{eq}}(r_\perp, r_\parallel = 0)$ in rectangular systems containing short stripes ($L_\perp \gg L_\parallel$). (a) The equilibrium correlation function is plotted as a function of the distance r_\perp for different system sizes L_\parallel . The equilibrium correlation length increases with L_\parallel . (b) The rescaled equilibrium correlation function $C_\theta^{\text{eq}}(r_\perp, r_\parallel = 0)L_\parallel$ is plotted as a function of the scaling variable r_\perp/L_\parallel^2 for different system sizes. The black line represents the analytical result given by Eq. (27).

for a noise strength $\sigma^2 = 0.008$, which we use throughout the rest of this work. We observe excellent agreement between theory and the numerical data, noting that the correlation function becomes independent of time for $t \gtrsim \tau_{\text{eq}}^\parallel$, where $\tau_{\text{eq}}^\parallel \equiv \frac{1}{2\nu_4}(L_\parallel/2\pi)^4 \approx 1.024 \times 10^4$ for $L_\parallel = 8\lambda_0$.

We note that the spatial correlation function [Eq. (25)] can be written in scaling form: $C_\theta(r_\perp, r_\parallel = 0, t) = f[\frac{r_\perp}{\xi_\perp(t)}, \frac{r_\perp}{\xi_\perp^\text{eq}}, \frac{t}{\tau_{\text{eq}}^\parallel}]$, where we identify the following quantities: the equilibration time $\tau_{\text{eq}}^\parallel$ according to Eq. (19), the time-dependent correlation length $\xi_\perp(t) \equiv \sqrt{8\nu_2 t}$, which we already encountered in our previous work [17], and the equilibrium correlation length

$$\xi_\perp^{\text{eq}} \equiv \lambda_p^{-1}(L_\parallel/2\pi)^2. \quad (26)$$

We now discuss the properties of $C_\theta(r_\perp, r_\parallel = 0, t)$ in more detail. The time t enters Eq. (25) solely through the arguments of the error functions $\text{erf}[g_1(t)]$ and $\text{erfc}[g_2(t)]$, with $g_1(t) \equiv \sqrt{nt/\tau_{\text{eq}}^\parallel} - r_\perp/\xi_\perp(t)$ and $g_2(t) \equiv \sqrt{nt/\tau_{\text{eq}}^\parallel} + r_\perp/\xi_\perp(t)$. Both functions diverge in the limit $t \rightarrow \infty$, causing the error functions to approach the constants 1 and 0, respectively. This marks the end of the temporal evolution. In comparison, it is easy to see that $\xi_\perp(t)$ represents the growing correlation length at early times, when the terms involving $\xi_\perp(t)$ are large. The crossover between these two behaviors is mediated by the time $\tau_{\text{eq}}^\parallel$ for both $g_1(t)$ and $g_2(t)$. The function $g_1(t)$ increases monotonously from the limit $g_1(t \rightarrow 0) = -\infty$, with a zero crossing at $t = t_0 = \sqrt{\tau_{\text{eq}}^\parallel/\nu_2} r_\perp$. $g_2(t)$ is strictly positive, with a global minimum also at $t = t_0$. Finally, in the limit $t \rightarrow \infty$, Eq. (25) reduces to

$$\begin{aligned} C_\theta^{\text{eq}}(r_\perp, r_\parallel = 0) &= \frac{4\sigma^2}{L_\parallel \sqrt{\nu_2 \nu_4}} \sum_{n=1}^{\infty} e^{-(q_n^\parallel)^2 \lambda_p r_\perp} \\ &= \frac{2\sigma^2}{L_\parallel \sqrt{\nu_2 \nu_4}} [\vartheta_3(0, e^{-r_\perp/\xi_\perp^{\text{eq}}}) - 1], \quad (27) \end{aligned}$$

where $\vartheta_3(\cdot, \cdot)$ is a Jacobi theta function. Equation (27) can be written in scaling form: $C_\theta^{\text{eq}}(r_\perp, r_\parallel = 0) \sim L_\parallel^{-1} f(r_\perp/L_\parallel^2)$, where $\xi_\perp^{\text{eq}} \sim L_\parallel^2$. We note that the first moment, which we use to extract the correlation length $\xi_\perp(t)$ from the numerical data, can be computed exactly for Eq. (27), resulting in $\tilde{\xi}_\perp^{\text{eq}} = \frac{\pi^2}{15} \xi_\perp^{\text{eq}}$. This quantity is represented by the dashed horizontal line in Fig. 3(b).

$C_\theta^{\text{eq}}(r_\perp, r_\parallel = 0)$ diverges as a power law $\sim r_\perp^{-1/2}$ for small values of r_\perp . This behavior compares to that of the spatial correlation function in an infinite system, where a power-law decay $\sim r_\perp^{-1/2}$ is observed in the limit $t \rightarrow \infty$ [17]. In contrast to the infinite system, the equilibrium correlation function given by Eq. (27) decreases exponentially ($\sim e^{-r_\perp/\xi_\perp^{\text{eq}}}$) as $r_\perp \rightarrow \infty$.

In Fig. 4(a) the equilibrium spatial correlation function $C_\theta^{\text{eq}}(r_\perp, r_\parallel = 0)$ is plotted for different system sizes L_\parallel , with $L_\perp = 384\lambda_0$. It is apparent that the correlation length perpendicular to the stripes increases as a function of L_\parallel . To confirm this and to compare the numerical data with the theoretical result [Eq. (27)], we multiplied $C_\theta^{\text{eq}}(r_\perp, r_\parallel = 0)$ by L_\parallel and plotted it as a function of the rescaled distance r_\perp/L_\parallel^2 [Fig. 4(b)]. The data from systems with different sizes L_\parallel collapse onto a single curve, thereby confirming the scaling form of Eq. (27), and even the shape of the scaling function is in excellent agreement with the theoretical prediction [Eq. (27)].

At this point, we note that the relation between the equilibrium correlation length and the system size $\xi_\perp^{\text{eq}} \sim L_\parallel^2$ [Eq. (26)] can be reproduced exactly if one utilizes de Gennes' argument (p. 354 in Ref. [12]) that a modulation along the stripe (layer) with wave number $k = 2\pi/L_\parallel$ is attenuated in the direction perpendicular to the stripes over a distance $1/k^2 \lambda_p$. This distance equals the equilibrium correlation length ξ_\perp^{eq} [Eq. (26)]. De Gennes has also shown [12,53] that fluctuations of the smectic layers, as detected by light scattering, result in a high intensity for wave numbers $\nu_2 q_\perp^2 < \nu_4 q_\parallel^4$ (in our notation), which expresses a similar relation of length scales parallel and perpendicular to the stripes [65].

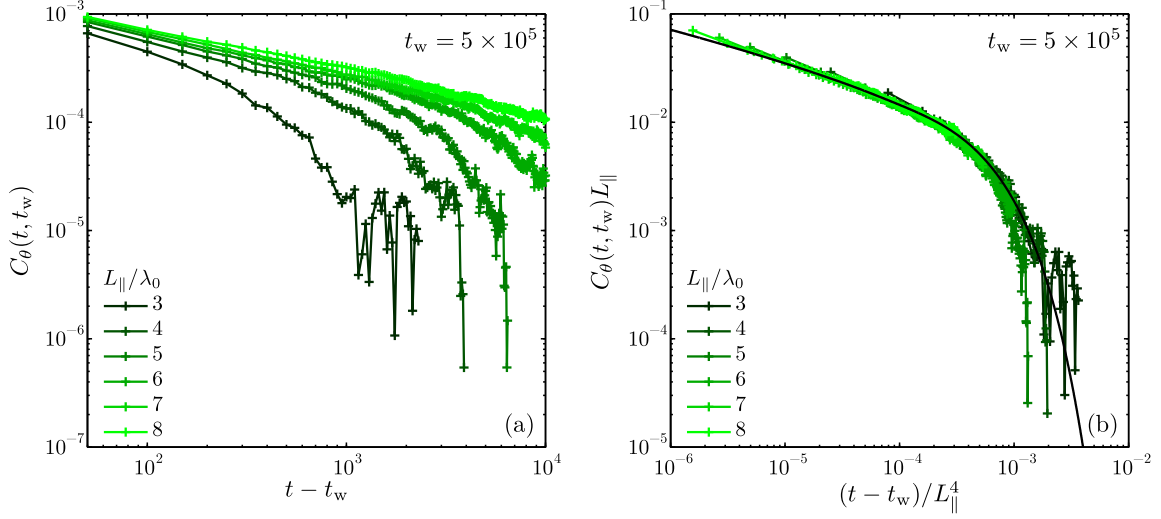


FIG. 5. Equilibrium behavior of the two-time correlation function $C_\theta(t, t_w)$ in systems containing short stripes. (a) $C_\theta(t, t_w)$ is plotted as a function of $t - t_w$ for different system sizes L_\parallel . The waiting time $t_w = 5 \times 10^5$. (b) The same data, rescaled by L_\parallel , are plotted as a function of $(t - t_w)/L_\parallel^4$. The black line represents Eq. (29).

We now turn to the temporal evolution of the orientation fluctuations in systems comprised of short stripes. To obtain the two-time correlation function $C_\theta(t, t_w)$, we replace the sum $\frac{1}{L_\perp} \sum_m$ in Eq. (23) by the integral $\frac{1}{2\pi} \int dq_\perp$:

$$C_\theta(t, t_w) = \frac{4\sigma^2}{L_\parallel \sqrt{v_2 v_4}} \sum_{n=1}^{\infty} \{ \text{erfc}[\sqrt{v_4 (q_n^\parallel)^4 (t - t_w)}] - \text{erfc}[\sqrt{v_4 (q_n^\parallel)^4 (t + t_w)}] \}. \quad (28)$$

$C_\theta(t, t_w)$ according to Eq. (28) is plotted for $L_\perp = 384\lambda_0$ and $L_\parallel = 3\lambda_0$ in the inset in Fig 3(c). The numerical data collapse for different waiting times and are well described by the theoretical prediction. As seen in the semilogarithmic plot, the decay of the two-time correlation function is rapid, but it is slightly different from a purely exponential decay.

Since the complementary error function in Eq. (28) decays rapidly for large arguments, the two-time correlation function $C_\theta(t, t_w)$ depends only on $t - t_w$ for $t_w \rightarrow \infty$:

$$C_\theta^{\text{eq}}(t - t_w) = \frac{4\sigma^2}{L_\parallel \sqrt{v_2 v_4}} \sum_{n=1}^{\infty} \text{erfc}[\sqrt{v_4 (q_n^\parallel)^4 (t - t_w)}]. \quad (29)$$

In this limit, the dynamics becomes time-translationally invariant as equilibrium is reached. Equation (29) can be written in the following scaling form: $C_\theta^{\text{eq}}(t - t_w) \sim \frac{1}{L_\parallel} f[(t - t_w)/2\tau_{\text{eq}}^\parallel]$, with the equilibration time $\tau_{\text{eq}}^\parallel$ as given in Eq. (19).

In Fig. 5 we take the theoretical predictions of Eq. (29), truncating the sum after 10^5 terms, and compare them with numerical data for a late waiting time $t_w = 5 \times 10^5$ and different system sizes L_\parallel . The size $L_\perp = 384\lambda_0$ is kept constant. In Fig. 5(a) $C_\theta(t, t_w)$ is plotted as a function of the difference $t - t_w$. The two-time correlation function decays more slowly as the system size L_\parallel is increased. While $C_\theta(t, t_w)$ resembles a power law in large systems, it behaves more like an exponential for small values of L_\parallel . In Fig. 5(b) we test the scaling properties of $C_\theta(t, t_w)$ by plotting the rescaled function $C_\theta(t, t_w)L_\parallel$ as a function of $(t - t_w)/L_\parallel^4$. We observe a collapse

of the data for different system sizes onto a master curve. Furthermore, there is excellent agreement with the theoretical prediction for $C_\theta^{\text{eq}}(t - t_w)$ [Eq. (29)].

To summarize, in finite systems with $L_\perp \gg L_\parallel$, the orientation dynamics, as represented by the two-time correlation function $C_\theta(t, t_w)$, becomes time-translationally invariant for long waiting times $t_w \gtrsim \tau_{\text{eq}}^\parallel$. This is a clear indication that the system has reached equilibrium. In equilibrium, $C_\theta^{\text{eq}}(t - t_w)$ decays similar to an exponential with a characteristic time scale $\tau_{\text{eq}}^\parallel$, which increases as the fourth power of the system size L_\parallel . The spatial orientation correlation function $C_\theta^{\text{eq}}(r_\perp, r_\parallel = 0)$ decays asymptotically as an exponential with the correlation length $\xi_\perp^{\text{eq}} = \lambda_p^{-1}(L_\parallel/2\pi)^2$. Last, the dominant modulation length λ_\parallel^* has reached the system size L_\parallel . Thus, we conclude that, once the elastic constants v_2 and v_4 are fixed, all equilibrium quantities are determined by L_\parallel .

B. Long stripes: $L_\perp \ll L_\parallel$

We now turn to the case $L_\perp \ll L_\parallel$, corresponding to systems containing a small number of long stripes. In Fig. 6(a) the characteristic length scales $\xi_\perp(t)$ and $\lambda_\parallel^*(t)$ are plotted as function of time for a system with $L_\perp = 8\lambda_0$ and $L_\parallel = 384\lambda_0$. The correlation length increases initially as $t^{1/2}$ and later approaches a constant value prescribed by the system size L_\perp . Since for $L_\perp = 8\lambda_0$, the crossover time $\tau_C^\perp = \frac{1}{2v_2}(L_\parallel/2\pi)^2 = 40$ [Eq. (18)], this coarsening dynamics corresponds to that of a quasi-1D system, as described below, whereas the dominant modulation length $\lambda_\parallel^*(t)$ grows as a power law $\sim t^{1/4}$, even at the latest times.

In Fig. 6(b) the two-time correlation function $C_\theta(t, t_w)$ is plotted as a function of $t - t_w$ for different waiting times t_w . $C_\theta(t, t_w)$ clearly depends on t_w , with the relaxation becoming slower and the magnitude becoming larger as the waiting time is increased. Thus, a system containing long stripes exhibits aging within the time range $t \leq 5 \times 10^5$ studied in our numerical simulations. This is expected, since the equilibration time $\tau_{\text{eq}}^\parallel = 5.4 \times 10^{10}$ for $L_\parallel = 384\lambda_0$.

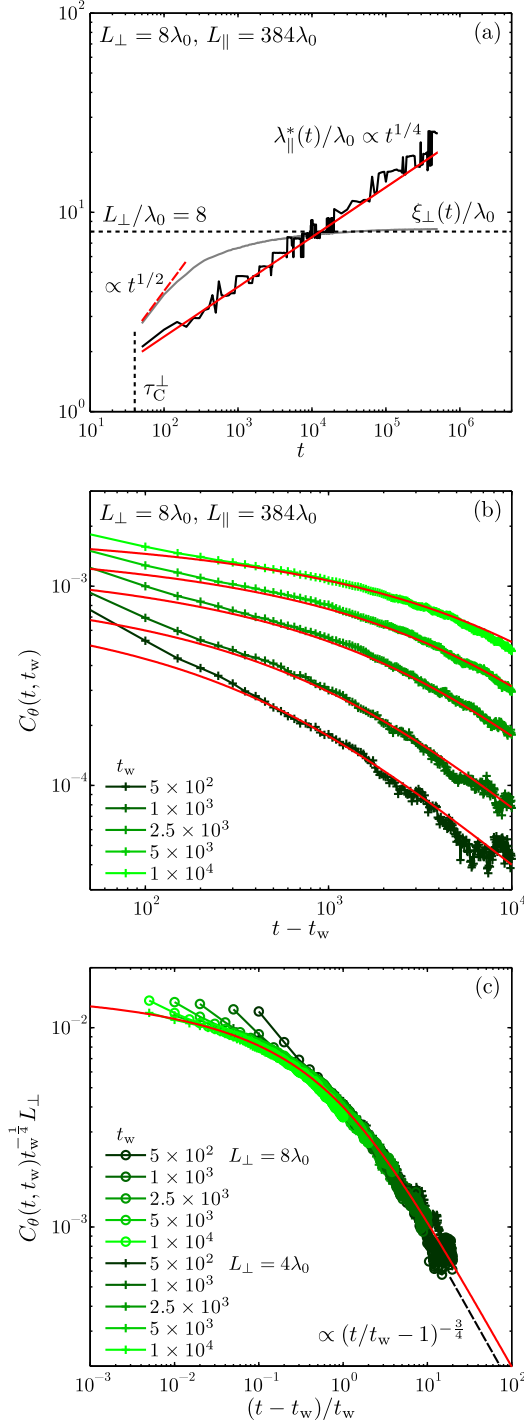


FIG. 6. Coarsening and aging in systems comprised of long stripes. (a) Growth of the length scales $\lambda_{\parallel}^*(t)$ and $\xi_{\perp}(t)$ for $L_{\perp} = 8\lambda_0$. The solid red line is a power law $\sim t^{1/4}$, indicating the ongoing growth of the dominant modulation length $\lambda_{\parallel}^*(t)$. The correlation length $\xi_{\perp}(t)$ approaches the system size L_{\perp} , indicated by the dashed horizontal line. The dashed vertical line represents the characteristic time τ_C^{\perp} [Eq. (18)]. (b) Aging dynamics in the same system. $C_{\theta}(t, t_w)$ is plotted as a function of the difference $t - t_w$. The solid red lines represent Eq. (31). (c) Scaling behavior of $C_{\theta}(t, t_w)$. The data for different system sizes and waiting times collapse onto a single curve upon rescaling. The solid red line represents the rescaled $C_{\theta}(t, t_w)$ according to Eq. (31). The dashed black line is a power law indicating the asymptotic behavior of the scaling function.

To explain these observations, we use the Landau-Peierls model to calculate the corresponding two-time correlation function. In the limit $L_{\parallel} \rightarrow \infty$, the sum $\frac{1}{L_{\parallel}} \sum_n$ in Eq. (23) can be replaced by the integral $\frac{1}{2\pi} \int dq_{\parallel}$. Carrying out the integration yields

$$I(t) = \frac{2\sigma^2}{\pi L_{\perp}} \left\{ \frac{\sqrt{2\pi}}{(v_2 v_4^3)^{1/4} \Gamma(\frac{1}{4})} \sum_{m=1}^{\infty} \frac{1}{\sqrt{q_m^{\perp}}} \Gamma\left[\frac{1}{4}, v_2 (q_m^{\perp})^2 t\right] - \frac{2\sqrt{2\pi}}{v_4^{3/4} \Gamma(\frac{1}{4})} t^{\frac{1}{4}} \right\}. \quad (30)$$

For $t \gg \tau_C^{\perp}$, the terms in the remaining sum over m are exponentially small and can therefore be neglected. In comparison, the magnitude of the second term in Eq. (30), which corresponds to pure bending fluctuations with $q_m^{\perp} = 0$, increases $\propto t^{\frac{1}{4}}$. This leads to the two-time correlation function

$$C_{\theta}(t, t_w) = \frac{4\sqrt{2}\sigma^2}{L_{\perp} v_4^{3/4} \Gamma(\frac{1}{4})} [(t + t_w)^{\frac{1}{4}} - (t - t_w)^{\frac{1}{4}}], \quad (31)$$

represented by the red lines in Fig. 6(b). Apart from small deviations for small time differences $t - t_w$, we observe excellent agreement between theory and the numerical data.

Apart from the prefactor, the result for $C_{\theta}(t, t_w)$ given in Eq. (31) is identical to the two-time correlation function obtained from the 1D Mullins-Herring equation with conserved noise (MHc) [61–63], namely, Eq. (12) in one spatial dimension with $v_2 = 0$. Equation (31) can be written in scaling form, $C_{\theta}(t, t_w) \sim t_w^{-b} f(t/t_w)$, where the aging exponent $b = -\frac{1}{4}$. This exponent can also be written as $b = -2\beta$ [66], with $\beta = \frac{1}{8}$, which is the growth exponent of the 1D MHc equation [41,61,62]. We note that $b = -\frac{1}{4} < 0$ indicates that the orientation fluctuations grow without bounds, leading to the destruction of orientational order. This stands in contrast to the infinite system, where $b = \frac{1}{4}$ [17], and orientational order is retained [26]. The scaling function characterizing $C_{\theta}(t, t_w)$ is given by $f(t/t_w) = (t/t_w + 1)^{\frac{1}{4}} - (t/t_w - 1)^{\frac{1}{4}}$. For large ratios $t/t_w \rightarrow \infty$, it decays as a power law $f(t/t_w) \sim (t/t_w)^{-\frac{3}{4}}$, which defines the autocorrelation exponent [31] $\lambda_C = \frac{3}{4}$.

The system size L_{\perp} appears only in the prefactor of Eq. (31). To test the corresponding finite-size behavior and the temporal scaling, we plotted the rescaled correlation function $C_{\theta}(t, t_w)t_w^{-1/4}L_{\perp}$ as a function of $t/t_w - 1$ in Fig. 6(c). The data for two different system sizes and multiple waiting times collapse onto a single curve, which is well described by the scaling function predicted by theory, $g(x) = (x + 2)^{\frac{1}{4}} - x^{\frac{1}{4}}$, with $x \equiv t/t_w - 1$. Asymptotically, $g(x)$ behaves as a power law $\sim x^{-\lambda_C}$ with the exponent $\lambda_C = \frac{3}{4}$. This power law is indicated by the dashed black line in Fig. 6(c).

For $t < \tau_{\text{eq}}^{\perp}$, aging is present even in systems with $L_{\perp} = \lambda_0$, corresponding to a single long stripe (data not shown). However, the magnitude of the correlation function $C_{\theta}(t, t_w)$ is smaller than predicted by theory for $L_{\perp} < 4\lambda_0$. This is likely due to an interplay of the stripe width λ_0 and the system size L_{\perp} . Such an effect is not accounted for by the Landau-Peierls

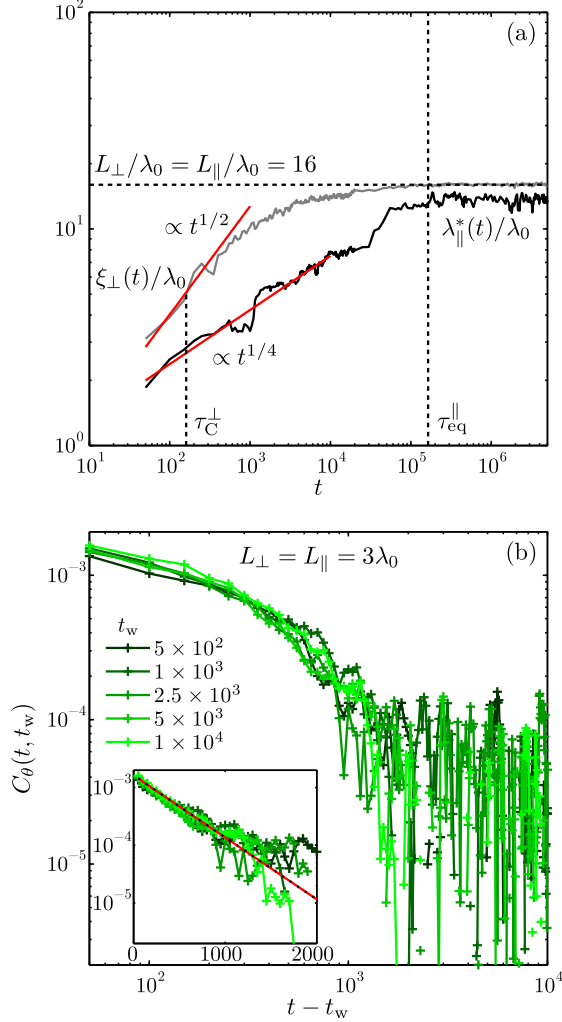


FIG. 7. Pathway to equilibrium in square systems. (a) Growth of the length scales $\lambda_{\parallel}^*(t)$ and $\xi_{\perp}(t)$ in a system with $L_{\perp} = L_{\parallel} = 16\lambda_0$. The corresponding characteristic times τ_C^{\perp} and $\tau_{\text{eq}}^{\parallel}$ are marked with vertical dashed lines. The dashed horizontal line indicates the system size, which limits the growth of both length scales. Note that $\tau_C^{\perp} \ll \tau_{\text{eq}}^{\parallel}$. (b) Equilibrium dynamics of the two-time correlation function for $L_{\perp} = L_{\parallel} = 3\lambda_0$, where $C_{\theta}^{\text{eq}}(t - t_w)$ depends only on the difference $t - t_w$. The inset shows the same data on a semilogarithmic scale. The solid red line is an exponential according to Eq. (33).

model, since the latter describes a coarse-grained orientation field $\theta(\mathbf{r}, t)$, not individual stripes.

C. Square systems: $L_{\perp} = L_{\parallel}$

Finally, we consider square systems with size $L_{\perp} = L_{\parallel}$, where the temporal evolution exhibits a transient behavior with features seen in systems with short stripes as well as those with long stripes. In Fig. 7(a) we plot the two characteristic length scales $\lambda_{\parallel}^*(t)$ and $\xi_{\perp}(t)$ for a system with $L_{\perp} = L_{\parallel} = 16\lambda_0$. Both quantities initially grow as power laws of time before approaching their equilibrium values at late times. Notably, the correlation length $\xi_{\perp}(t)$ exhibits signs of saturation several decades earlier in time than the dominant modulation length $\lambda_{\parallel}^*(t)$. The reason for this behavior is that $\tau_C^{\perp} = 1.60 \times 10^2 \ll$

$\tau_{\text{eq}}^{\parallel} = 1.64 \times 10^5$ for $L_{\perp} = L_{\parallel} = 16\lambda_0$ [Eqs. (18) and (19)]. At $t = \tau_C^{\perp}$, the system displays a crossover to the dynamics of a quasi-1D system. For $\tau_C^{\perp} < t < \tau_{\text{eq}}^{\parallel}$, the observed growth of the dominant modulation length $\lambda_{\parallel}^*(t)$ is described by the 1D MHC equation. At $t = \tau_{\text{eq}}^{\parallel}$, the system reaches equilibrium.

In Fig. 7(b) the two-time correlation function is plotted as a function of $t - t_w$ for a smaller system with $L_{\perp} = L_{\parallel} = 3\lambda_0$, which reaches equilibrium at earlier times than the one considered before. $C_{\theta}(t, t_w)$ is independent of the waiting time t_w within the range of times considered here, which indicates equilibrium dynamics. In the inset, the same data are plotted on a semilog scale, showing that the decay of the correlation function is consistent with an exponential.

This equilibrium behavior can also be explained using the Landau-Peierls model. The two-time correlation function $C_{\theta}(t, t_w)$ is given by Eq. (23), where we now consider both L_{\perp} and L_{\parallel} , to be finite. Since all terms appearing in Eq. (23) are weighted with an exponential that decays rapidly for large indices m and n , we can approximate $I(t)$ by retaining only those terms corresponding to $m, n \leq 1$:

$$I(t) \approx 4\sigma^2 \left\{ \frac{4L_{\perp}^2 L_{\parallel}^2}{v_2 L_{\parallel}^4 + 4v_4 \pi^2 L_{\perp}^2} e^{-[v_2(2\pi/L_{\perp})^2 + v_4(2\pi/L_{\parallel})^4]t} + \frac{1}{2v_4 \pi^2} e^{-v_4(2\pi/L_{\parallel})^4 t} \right\} \approx \frac{2\sigma^2}{v_4 \pi^2} e^{-v_4(2\pi/L_{\parallel})^4 t}. \quad (32)$$

At late times t , the only relevant term is the second one in Eq. (32), since the first term is exponentially smaller. Finally, we arrive at the following expression for the equilibrium two-time correlation function, valid for waiting times $t_w \gg t - t_w$, where $I(t + t_w)$ is negligible:

$$C_{\theta}^{\text{eq}}(t - t_w) = \frac{2\sigma^2}{v_4 \pi^2} e^{-(t-t_w)/2\tau_{\text{eq}}^{\parallel}}. \quad (33)$$

Clearly, $C_{\theta}^{\text{eq}}(t - t_w)$ is time-translationally invariant, since it depends only on the difference $t - t_w$. The exponential in Eq. (33) decays with a time constant $2\tau_{\text{eq}}^{\parallel}$. $C_{\theta}^{\text{eq}}(t - t_w)$ is plotted as a dotted black line in the inset in Fig. 7(b). This approximate result can be compared to a numerical evaluation of the exact correlation function [Eq. (32)], which is plotted as a solid red line in the inset. The differences are insignificant, thus justifying our assumptions leading to Eq. (33).

We now turn to the dynamics of the structure factor $S_{\theta}(q_m^{\perp} = 0, q_n^{\parallel}, t)$, which represents the behavior of the undulation modes in the direction of the stripes. As opposed to an infinite system, where q_{\parallel} is continuous, there are only discrete wave numbers in a finite system. Therefore, the wave number $q_{\parallel}^*(t)$ corresponding to the peak position cannot become smaller than the wave number $2\pi/L_{\parallel}$ determined by system size L_{\parallel} . Setting $q_{\parallel}^*(t) = 2\pi/L_{\parallel}$ yields the characteristic time $\tau_0 \equiv \frac{c_0}{2v_4} (L_{\parallel}/2\pi)^4 = c_0 \tau_{\text{eq}}^{\parallel}$ (with $c_0 \approx 1.2564$, as given in Sec. III B). At $t = \tau_0$, the position of the maximum $S_{\theta}^*(t)$ reaches the smallest possible wave number. This compares to the time $\tau_{\text{eq}}^{\parallel}$ when the exponential in Eq. (21) has decreased by a factor of e^{-1} for the smallest wave number $q_{\parallel}^{\parallel} = 2\pi/L_{\parallel}$.

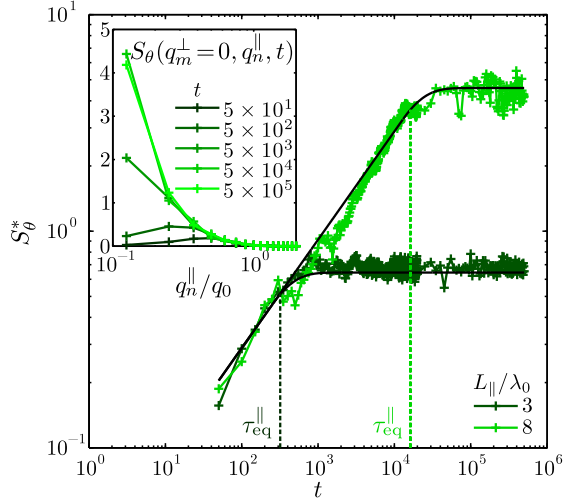


FIG. 8. Growth and saturation of the peak intensity $S_\theta^*(t)$ in small square systems. The continuous black lines represent the theoretical result [Eq. (34)], while the dashed lines indicate the equilibration time $\tau_{\text{eq}}^{\parallel}$. The inset shows the evolution of the structure factor $S_\theta(q_m^\perp = 0, q_n^\parallel, t)$ for the system with $L_\perp = L_\parallel = 8\lambda_0$.

The peak intensity in a finite system can thus be written as a piecewise-defined but continuous function

$$S_\theta^*(t) = \begin{cases} \frac{\sigma^2}{\pi^2 c_1 v_4} L_\parallel^2 \sqrt{t/\tau_0}, & t \leq \tau_0, \\ \frac{\sigma^2}{\pi^2 v_4} L_\parallel^2 [1 - e^{-c_0 t/\tau_0}], & t > \tau_0, \end{cases} \quad (34)$$

representing a power-law increase $\sim t^{\frac{1}{2}}$ at early times $t \leq \tau_0$, followed by an exponential approach to the equilibrium value $S_\theta^{*,\text{eq}} \equiv S_\theta(q_m^\perp = 0, 2\pi/L_\parallel, \infty) = \frac{\sigma^2}{\pi^2 v_4} L_\parallel^2$ at late times $t > \tau_0$. We test the predictions from Eq. (34) in Fig. 8. The inset demonstrates the evolution of the entire structure factor $S_\theta(q_\perp = 0, q_\parallel, t)$, which is characterized by a shift of the peak position towards the smallest wave number, as well as an increase in the peak intensity. In the main panel, the peak intensity $S_\theta^*(t)$ is plotted as a function of time for two systems with $L_\perp = L_\parallel = 3\lambda_0$ and $8\lambda_0$, respectively. In both cases, $S_\theta^*(t)$ first grows as a power law and approaches an equilibrium value at late times. This dependency, including the crossover to equilibrium controlled by $\tau_{\text{eq}}^{\parallel}$, is well described by Eq. (34).

The peak intensity $S_\theta^*(t)$ can be written in a scaling form equivalent to the Family-Vicsek scaling [42] observed in surface roughening phenomena [41,59]:

$$S_\theta^*(t) \sim L_\parallel^{2\alpha+1} \hat{g}(t/L_\parallel^z), \quad (35)$$

with the scaling exponents $\alpha = \frac{1}{2}$ and $z = 4$ related by $\alpha/\beta = z$. Therefore, examining data from finite systems provides access to the exponent α and complements our study of the dynamics in infinite systems [17]. We note that the growth exponent α can also be extracted from the power-law decay of the equilibrium structure factor [62], where $S_\theta^{\text{eq}}(q_m^\perp = 0, q_n^\parallel) = \frac{4\sigma^2}{v_4(q_n^\parallel)^2} \propto (q_n^\parallel)^{-2\alpha-1}$ is the limit $t \rightarrow \infty$ of Eq. (21). Since a cut through the structure factor $S_\theta(q_m^\perp = 0, q_n^\parallel, t)$ is only sensitive to the system size L_\parallel , the extension perpendicular to the stripes L_\perp is not expected to influence the scaling behavior.

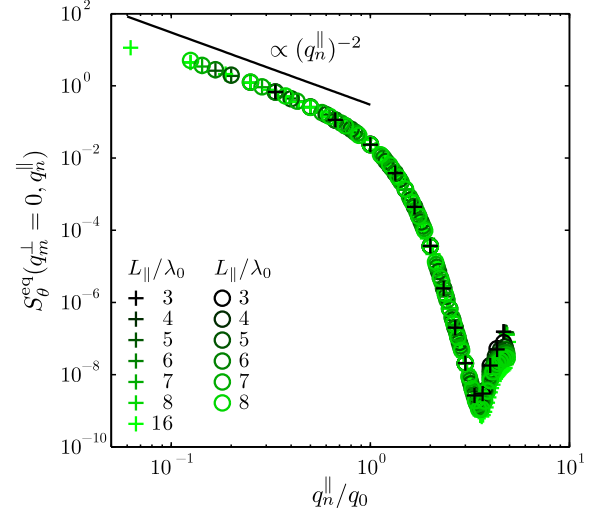


FIG. 9. Common scaling behavior of the structure factor $S_\theta^{\text{eq}}(q_m^\perp = 0, q_n^\parallel)$ in small square systems (+) and systems containing many short stripes (\circ). The black line represents a power law drawn to illustrate the scaling behavior at small wave numbers q_n^\parallel .

In Fig. 9 the equilibrium structure factor $S_\theta^{\text{eq}}(q_m^\perp = 0, q_n^\parallel)$ is plotted for both small square systems and rectangular systems with $L_\perp \gg L_\parallel$. In the latter case, the system size L_\parallel parallel to the stripes was varied, while $L_\perp = 384\lambda_0$ was kept constant. For small wave numbers $q_\parallel/q_0 \lesssim 1$, the structure factor exhibits power-law behavior $\propto q_\parallel^{-2}$. At large wave numbers $q_\parallel/q_0 \gtrsim 1$, a much faster decay is observed, which coincides with the range where the time-dependent structure factor shows no evolution [17]. It is easy to see that the shape of $S_\theta^{\text{eq}}(q_m^\perp = 0, q_n^\parallel)$ does not change as a function of the system size. Furthermore, the data points for square and rectangular systems overlap each other. However, the larger the system size L_\parallel , the smaller the minimal wave number $2\pi/L_\parallel$, and thus the range in which the structure factor exhibits the power law increases with the system size.

To further investigate the dynamics and the scaling behavior in both square and rectangular systems, we have plotted the equilibrium peak intensity $S_\theta^{*,\text{eq}}$ as a function of L_\parallel in Figs. 10(a) and 10(c). In both cases, $S_\theta^{*,\text{eq}}$ increases as the square of the respective system size, leading to the exponent $\alpha = \frac{1}{2}$ according to Eq. (35). Only the intensity for the square system with $L_\parallel = 16\lambda_0$ falls slightly short of the value expected from theory.

Finally, we plot the numerical data in scaling form according to Eq. (35). This is shown in Figs. 10(b) and 10(d), where a collapse onto the same master curve is observed after rescaling the intensity by L_\parallel^2 and the time by L_\parallel^4 . This confirms the functional dependence of the structure factor on the system size L_\parallel , with the exponents $\alpha = \frac{1}{2}$ and $z = 4$ in agreement with the values obtained in Ref. [17]. We note that the divergence of the equilibration time $\tau_{\text{eq}}^{\parallel} \sim L_\parallel^z$ is consistent with the growth of the dominant modulation length $\lambda_\parallel^*(t) \sim t^{\frac{1}{z}}$ observed here and in our previous work, indicating that a single exponent z determines the behavior of the time scale and the length scale. The system size L_\parallel controls the equilibration of S_θ^* by limiting

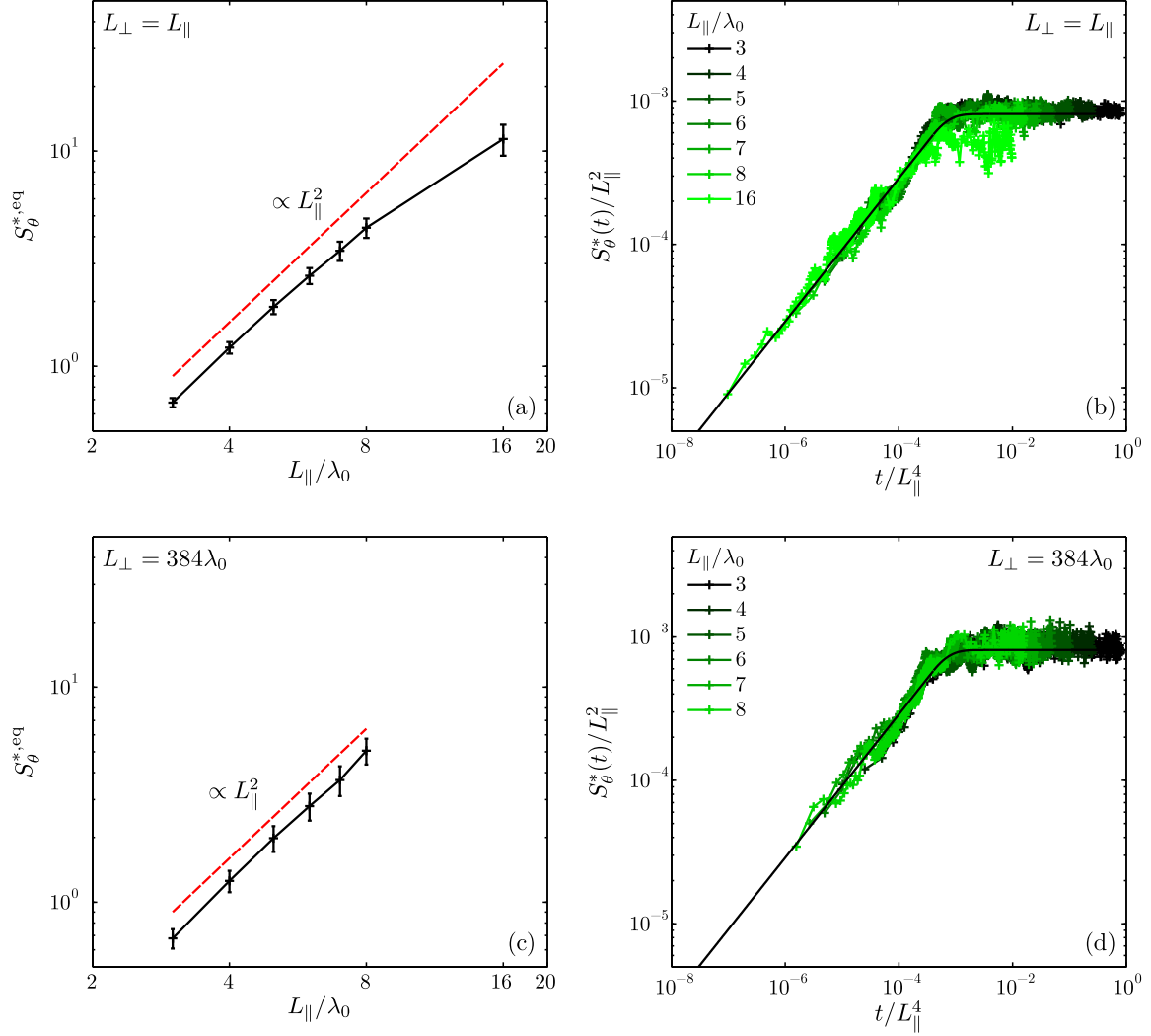


FIG. 10. Finite-size scaling of the peak intensity S_θ^* in (a), (b) square systems and (c), (d) rectangular systems consisting of short stripes. In (a) and (c), the equilibrium value $S_\theta^{*,eq}$ is plotted as a function of the system sizes L_\parallel . The dashed red lines represent a power law. In (b) and (d), the peak intensity $S_\theta^*(t)$ has been rescaled, demonstrating a scaling collapse for different system sizes. The black lines represent Eq. (34).

the dominant modulation length λ_\parallel^* and therefore the length scale of the orientation fluctuations parallel to the stripes.

V. CONCLUSIONS

In Fig. 11 we give an overview of the different system sizes for which we performed simulations of the phase-field model for a stripe-forming system. The equilibration time τ_{eq}^\parallel [Eq. (19)] grows as the fourth power of L_\parallel and is represented by dashed vertical lines in Fig. 11. This restricts the size of the systems for which equilibrium could be attained within the time range $t \leq 5 \times 10^6$ of our numerical simulations. Systems which reached equilibrium are indicated by closed circles in Fig. 11, whereas open circles indicate systems which remained out of equilibrium. Another way to differentiate systems of finite size involves the condition $\tau_C^\perp < \tau_{eq}^\parallel$, which is met by systems with $(L_\perp/\lambda_0) < 2(L_\parallel/\lambda_0)^2$. This condition is represented by the solid red line in Fig. 11 (in our case, $\lambda_p = \lambda_0/4\pi$). In the systems located below this line, the dynamics switches at $t = \tau_C^\perp$ from initially unperturbed aging

and coarsening (comparable to that of an infinite 2D system) to the aging and coarsening dynamics of a quasi-1D system described by the 1D MHC equation [61–63], before reaching equilibrium at $t = \tau_{eq}^\parallel$. The systems above the solid red line approach the equilibrium directly. This pathway is taken by systems containing short stripes. We refer to this pathway as 2D equilibration behavior in contrast to the pathway to equilibrium via the 1D MHC behavior.

The condition $L_\perp < L_\parallel^2/2\pi\lambda_p$ is equivalent to the condition $L_\perp < 2\pi\xi_\perp^{eq}$. In these systems, the equilibrium correlation length ξ_\perp^{eq} would be close to or larger than L_\perp . Thus, at sufficiently late times, the orientation fluctuations are correlated across the entire system width, corroborating the notion of quasi-1D behavior. This scenario is realized in systems containing long stripes. We note that the large square system with $L_\perp = L_\parallel = 55\lambda_0$ studied numerically in Ref. [17] also falls into this regime, since $\tau_C^\perp = 1.89 \times 10^3$ and $\tau_{eq}^\parallel = 2.29 \times 10^7$. Therefore $\xi_\perp(t)$ exceeds the system size L_\perp at late times, but the system does not reach equilibrium within the time range studied in Ref. [17].

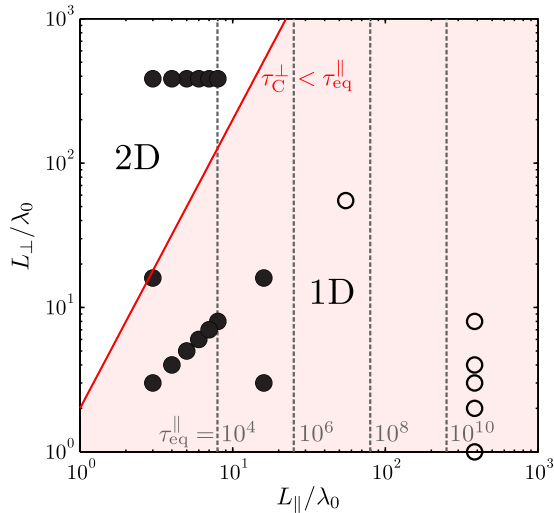


FIG. 11. Map of the pathways to equilibrium. Closed (open) circles indicate that equilibrium was reached (not reached) in numerical simulations of Eq. (3). The dashed vertical lines represent the equilibration time $\tau_{\text{eq}}^{\parallel}$ for a given value of L_{\parallel} . The solid red line represents the condition $\tau_{\text{C}}^{\perp} < \tau_{\text{eq}}^{\parallel}$. Systems located below this line approach equilibrium via the 1D MHC behavior. Systems above the solid red line display 2D equilibration behavior.

Our results show that orientation fluctuations in finite stripe phases with periodic boundary conditions approach equilibrium along different pathways, depending on the system sizes L_{\perp} and L_{\parallel} , their aspect ratio, and the undulation penetration length λ_p as shown in Fig. 11. All systems reach

equilibrium and display finite-size scaling of the characteristic times τ_{C}^{\perp} and $\tau_{\text{eq}}^{\parallel}$, as well as the length scales given by the equilibrium correlation length ξ_{\perp}^{eq} and the dominant modulation length λ_{\parallel}^* . Furthermore, we demonstrate finite-size scaling of the two-time correlation function $C_{\theta}(t, t_w)$, the structure factor $S_{\theta}^{\text{eq}}(q_m^{\perp} = 0, q_n^{\parallel})$, and the spatial correlation function $C_{\theta}^{\text{eq}}(r_{\perp}, r_{\parallel} = 0)$. In all cases, we find excellent agreement between our numerical results and the analytical predictions based on the Landau-Peierls model for the stripe orientation. In particular, the scaling of the structure factor $S_{\theta}^{\text{eq}}(q_m^{\perp} = 0, q_n^{\parallel})$ corresponds to the universality class of the 1D MHC equation, as shown for an infinite system in Ref. [17].

We expect that the presented methodology, namely, the extraction of the orientation field and the study of its correlation functions, can be used for characterizing the dynamics of stripe phases in other types of confinement, particularly in the case of no-flux boundary conditions (solid walls) [67,68]. Such conditions are often realized in experimental studies on block copolymer thin films [69–72]. Furthermore, the Landau-Peierls model is also applicable to lamellae-forming systems and smectic liquid crystals in three spatial dimensions [12]. The equilibrium behavior of undulation fluctuations in liquid crystals has been studied extensively theoretically and experimentally [12,20]. However, the pathways to equilibrium, especially starting from a perfectly ordered state, as well as anharmonic effects of thermal fluctuations that cause a breakdown of linear elasticity theory [73–75], remain to be explored.

ACKNOWLEDGMENTS

G.R. thanks J. Toner for inspiring discussions.

-
- [1] M. Seul and R. Wolfe, *Phys. Rev. A* **46**, 7519 (1992).
 - [2] A. B. Kashuba and V. L. Pokrovsky, *Phys. Rev. B* **48**, 10335 (1993).
 - [3] K. De’Bell, A. B. MacIsaac, and J. P. Whitehead, *Rev. Mod. Phys.* **72**, 225 (2000).
 - [4] O. Portmann, A. Vaterlaus, and D. Pescia, *Nature (London)* **422**, 701 (2003).
 - [5] E. Bodenschatz, W. Pesch, and G. Ahlers, *Annu. Rev. Fluid Mech.* **32**, 709 (2000).
 - [6] M. Lappa, *Thermal Convection: Patterns, Evolution and Stability* (Wiley, Chichester, 2010).
 - [7] M. J. Fasolka and A. M. Mayes, *Annu. Rev. Mater. Res.* **31**, 323 (2001).
 - [8] M. Seul and D. Andelman, *Science* **267**, 476 (1995).
 - [9] I. W. Hamley, *The Physics of Block Copolymers* (Oxford University Press, Oxford, 1998).
 - [10] J. M. Seddon and R. H. Templer, *Philos. Trans. Phys. Sci. Eng.* **344**, 377 (1993).
 - [11] C. E. Conn, O. Ces, X. Mulet, S. Finet, R. Winter, J. M. Seddon, and R. H. Templer, *Phys. Rev. Lett.* **96**, 108102 (2006).
 - [12] P.-G. de Gennes and J. Prost, *The Physics of Liquid Crystals*, Internat. Ser. Monogr. Phys., Vol. 83 (Clarendon Press, Oxford, 1995).
 - [13] R. Shlomovitz, L. Maibaum, and M. Schick, *Biophys. J.* **106**, 1979 (2014).
 - [14] V. J. Emery, S. A. Kivelson, and J. M. Tranquada, *Proc. Natl. Acad. Sci. USA* **96**, 8814 (1999).
 - [15] S. A. Kivelson, I. P. Bindloss, E. Fradkin, V. Oganesyan, J. M. Tranquada, A. Kapitulnik, and C. Howald, *Rev. Mod. Phys.* **75**, 1201 (2003).
 - [16] C. Riesch, G. Radons, and R. Magerle, *Phys. Rev. E* **90**, 052101 (2014).
 - [17] C. Riesch, G. Radons, and R. Magerle, *Interface Focus* **7**, 20160146 (2017).
 - [18] R. Peierls, *Ann. Inst. Henri Poincaré* **5**, 177 (1935).
 - [19] L. D. Landau, *Zh. Eksp. Teor. Fiz.* **7**, 627 (1937), English translation in *Collected Papers of L. D. Landau* (Pergamon Press, Oxford, 1965), p. 209.
 - [20] W. H. de Jeu, B. I. Ostrovskii, and A. N. Shalaginov, *Rev. Mod. Phys.* **75**, 181 (2003).
 - [21] L. D. Landau and E. M. Lifshitz, *Statistical Physics* (Pergamon Press, Oxford, 1959).
 - [22] W. Helfrich, *Appl. Phys. Lett.* **17**, 531 (1970).
 - [23] J. P. Hurault, *J. Chem. Phys.* **59**, 2068 (1973).
 - [24] M. Delaye, R. Ribotta, and G. Durand, *Phys. Lett. A* **44**, 139 (1973).

- [25] N. A. Clark and R. B. Meyer, *Appl. Phys. Lett.* **22**, 493 (1973).
- [26] J. Toner and D. R. Nelson, *Phys. Rev. B* **23**, 316 (1981).
- [27] M. E. Fisher and M. N. Barber, *Phys. Rev. Lett.* **28**, 1516 (1972).
- [28] V. Privman, ed., *Finite Size Scaling and Numerical Simulation of Statistical Systems* (World Scientific, Singapore, 1990).
- [29] K. Binder, in *Computational Methods in Field Theory*, Lecture Notes in Physics, Vol. 409, edited by H. Gausterer and C. Lang (Springer, Berlin, 1992), pp. 59–125.
- [30] A. J. Bray, *Adv. Phys.* **43**, 357 (1994).
- [31] M. Henkel and M. Pleimling, *Non-equilibrium Phase Transitions*, Vol. 2 (Springer, Dordrecht, 2010).
- [32] J. Viñals and D. Jasnow, *Phys. Rev. B* **37**, 9582 (1988).
- [33] H. Guo, Q. Zheng, and J. D. Gunton, *Phys. Rev. B* **38**, 11547 (1988).
- [34] N. Wilding, C. Munkel, and D. W. Heermann, *Z. Phys. B* **94**, 301 (1994).
- [35] S. K. Das, M. E. Fisher, J. V. Sengers, J. Horbach, and K. Binder, *Phys. Rev. Lett.* **97**, 025702 (2006).
- [36] S. Majumder and S. K. Das, *Phys. Rev. E* **81**, 050102 (2010).
- [37] S. Majumder and S. K. Das, *Phys. Rev. E* **84**, 021110 (2011).
- [38] S. K. Das, S. Roy, S. Majumder, and S. Ahmad, *Europhys. Lett.* **97**, 66006 (2012).
- [39] J. Midya, S. Majumder, and S. K. Das, *J. Phys.: Cond. Mat.* **26**, 452202 (2014).
- [40] A. Mendoza-Coto, D. A. Stariolo, and L. Nicolao, *Phys. Rev. Lett.* **114**, 116101 (2015).
- [41] A.-L. Barabási and E. H. Stanley, *Fractal Concepts in Surface Growth* (Cambridge University Press, Cambridge, 1995).
- [42] F. Family and T. Vicsek, *J. Phys. A: Math. Gen.* **18**, L75 (1985).
- [43] P. C. Hohenberg and B. I. Halperin, *Rev. Mod. Phys.* **49**, 435 (1977).
- [44] T. Ohta and K. Kawasaki, *Macromolecules* **19**, 2621 (1986).
- [45] J. G. E. M. Fraaije, *J. Chem. Phys.* **99**, 9202 (1993).
- [46] G. H. Fredrickson, V. Ganesan, and F. Drolet, *Macromolecules* **35**, 16 (2002).
- [47] J. J. Christensen, K. Elder, and H. C. Fogedby, *Phys. Rev. E* **54**, R2212 (1996).
- [48] J. J. Christensen and A. J. Bray, *Phys. Rev. E* **58**, 5364 (1998).
- [49] L. Q. Chen and J. Shen, *Comput. Phys. Commun.* **108**, 147 (1998).
- [50] J. Bigün and G. H. Granlund, in *Proceedings of the IEEE First International Conference on Computer Vision* (IEEE Computer Society, Washington, DC, 1987), pp. 433–438.
- [51] M. Kass and A. Witkin, *Comput. Vis. Graph. Image Process.* **37**, 362 (1987).
- [52] J. v. d. Weijer, L. J. v. Vliet, P. W. Verbeek, and M. v. Ginkel, *IEEE Trans. Pattern Anal. Mach. Intell.* **23**, 1035 (2001).
- [53] P. G. de Gennes, *J. Phys. Colloques* **30**, C4-65 (1969).
- [54] R. Graham, *Phys. Rev. A* **10**, 1762 (1974).
- [55] K. R. Elder, J. Viñals, and M. Grant, *Phys. Rev. A* **46**, 7618 (1992).
- [56] S. Qi and Z.-G. Wang, *J. Chem. Phys.* **111**, 10681 (1999).
- [57] Z. Wang, *J. Chem. Phys.* **100**, 2298 (1994).
- [58] P. de Gennes, *Solid State Commun.* **10**, 753 (1972).
- [59] J. Krug, *Adv. Phys.* **46**, 139 (1997).
- [60] H. Risken, *The Fokker-Planck Equation*, 2nd ed. (Springer, Berlin, 1996).
- [61] Z. Rácz, M. Siegert, D. Liu, and M. Plischke, *Phys. Rev. A* **43**, 5275 (1991).
- [62] J. G. Amar, P.-M. Lam, and F. Family, *Phys. Rev. E* **47**, 3242 (1993).
- [63] J. M. Kim, *Mod. Phys. Lett. B* **18**, 11 (2004).
- [64] R. M. Corless and D. J. Jeffrey, in *The Princeton Companion to Applied Mathematics*, edited by N. J. Higham, M. R. Dennis, P. Glendinning, P. A. Martin, F. Santosa, and J. Tanner (Princeton University Press, Princeton, 2015), pp. 151–155.
- [65] We thank J. Toner for pointing this out to us.
- [66] A. Röthlein, F. Baumann, and M. Pleimling, *Phys. Rev. E* **74**, 061604 (2006).
- [67] G. Brown and A. Chakrabarti, *J. Chem. Phys.* **101**, 3310 (1994).
- [68] V. Weith, A. Krekhov, and W. Zimmermann, *J. Chem. Phys.* **139**, 054908 (2013).
- [69] M. R. Hammond and E. J. Kramer, *Macromolecules* **39**, 1538 (2006).
- [70] Q. Tong and S. J. Sibener, *Macromolecules* **46**, 8538 (2013).
- [71] H. J. Ryu, Q. Tong, and S. J. Sibener, *J. Phys. Chem. Lett.* **4**, 2890 (2013).
- [72] V. Mishra and E. J. Kramer, *Macromolecules* **46**, 977 (2013).
- [73] G. Grinstein and R. A. Pelcovits, *Phys. Rev. Lett.* **47**, 856 (1981).
- [74] G. F. Mazenko, S. Ramaswamy, and J. Toner, *Phys. Rev. A* **28**, 1618 (1983).
- [75] L. Golubović and Z.-G. Wang, *Phys. Rev. Lett.* **69**, 2535 (1992).